O3M SAF Validation REPORT

Validated products:

Identifier	Name	Acronym
O3M-12	Offline total H_2O, GOME-2/MetOp-A	MAG-O-H2O
O3M-86	Offline total H_2O, GOME-2/MetOp-B	MBG-O-H2O
O3M-121	Reprocessed total H_2O, GOME-2/MetOp-A & B	MxG-RP1-H2O

Total H_2O Vertical Column GOME-2B, 10.04.2013

H_2O column density [kg/m^2]
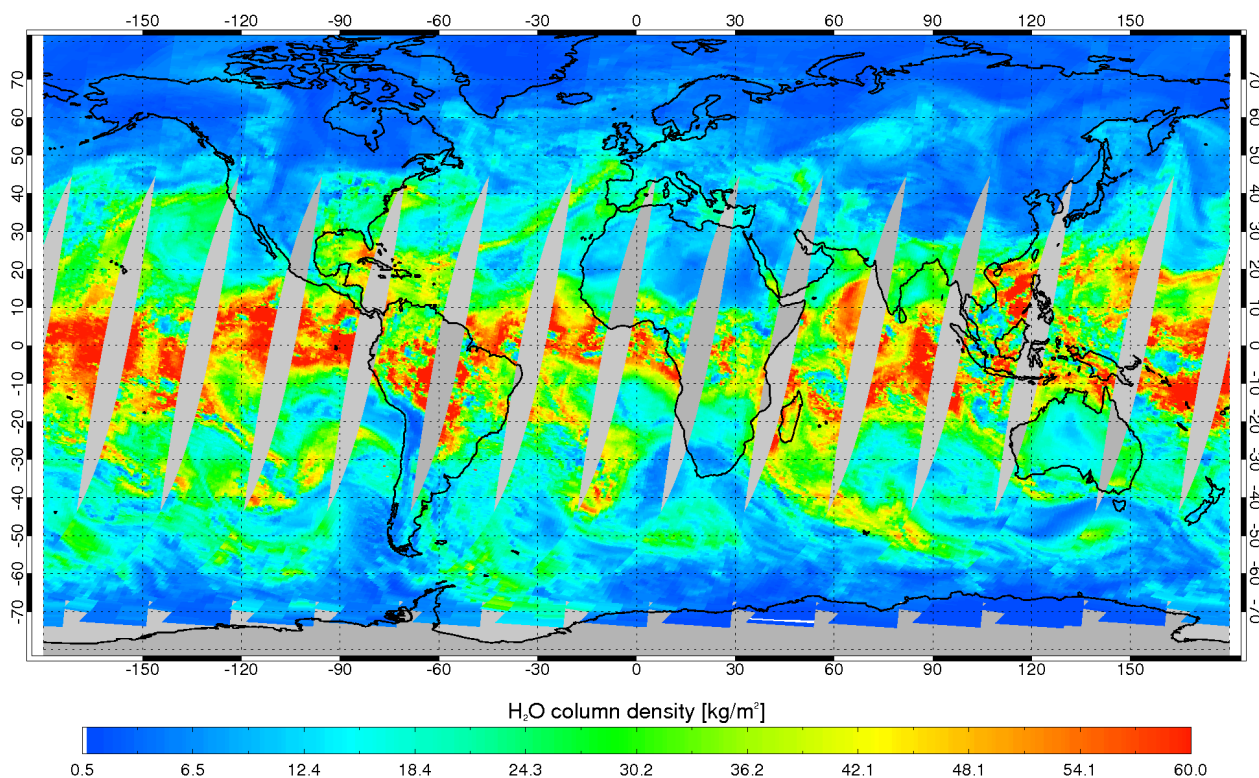
Authors:

Name	Institute
Margherita Grossi	Institut für Methodik der Fernerkundung (IMF), DLR
Niilo Kalakoski	Finnish Meteorological Institute
Pieter Valks	Institut für Methodik der Fernerkundung (IMF), DLR

Reporting period: GOME-2/MetOp-A Jan 2007 – August 2015

GOME-2/MetOp-B Jan 2013 – August 2015

Input data versions: GOME-2 Level 1B version 5.3.0 until 17 June 2014

GOME-2 Level 1B version 6.0.0 since 17 June 2014

Data processor versions: GDP 4.8, UPAS version 1.3.9

distribution

Function	Organisation
O3M-SAF	EUMETSAT, BIRA-IASB, DLR, DMI, DWD, FMI, AUTH, KNMI, LATMOS, RMI

document change record

Issue	Rev.	Date	Section	Description of Change
1	0	15.08.2015	all	Creation of this document

Validation report of GOME-2 offline and reprocessed H₂O column data from MetOp-A and MetOp-B

CONTENTS

ACRONYMS AND ABBREVIATIONS

AMF	Air Mass Factor
BRDF	Bidirectional Reflectance Distribution Function
DLR	German Aerospace Centre
FMI	Finnish Meteorological Institute
DOAS	Differential Optical Absorption Spectroscopy
ESA	European Space Agency
EUMETSAT	European Organisation for the Exploitation of Meteorological Satellites
GDP	GOME Data Processor
GOME	Global Ozone Monitoring Experiment
GOME-2A	GOME-2/MetOp-A
GOME-2B	GOME-2/MetOp-B
H_2O	Water Vapour
IMF	Remote Sensing Technology Institute
ITCZ	Intertropical Convergence Zone
LOS	Line Of Sight
NIR	Near Infrared
O3M-SAF	Ozone and Atmospheric Chemistry Monitoring Satellite Application Facility
REMSS	Remote Sensing System
RMSE	Root Mean Square Error
SAD	Scan Angle Dependency
SCD	Slant Column Density
SSD	Service Specification Document
SSMIS	Special Sensor Microwave Imager Sounder
SZA	Solar Zenith Angle
TCWV	Total Column Water Vapour
UPAS	Universal Processor for UV/VIS Atmospheric Spectrometers
VIS	Visible
VCD	Vertical Column Density

1. INTRODUCTION

1.1   Purpose and scope

The purpose of this document is to present the verification and the validation of EUMETSAT Satellite Application Facility on Atmospheric Chemistry Monitoring (O3M SAF) MetOp-A and MetOp-B offline and reprocessed GOME-2 H_2O total column data generated by DLR using the GOME Data Processor (GDP) version 4.8. The GOME-2 MetOp-A and MetOp-B data sets are available over the time period January 2007-March 2015 and December 2012-March 2015, respectively. The knowledge of the effective distribution of the total column water vapour (TCWV) is fundamental for weather monitoring as well as for the evaluation of climate models. Advancing in understanding of variability and changes in water vapor is vital, especially considering that, in contrast to most other greenhouse gases, the H_2O distribution is highly variable.

The overall consistency between measurements from the newer GOME-2 instrument on board of the MetOp-B platform and the GOME-2/MetOp-A data is evaluated in the overlap period December 2012 – March 2015. It is important to assess the accuracy and improve the post processing of satellite data in order to have a consistent picture of the coherence of the results produced employing different technologies.

A global validation of the GOME-2/MetOp-A and GOME-2/MetOp-B TCWV product presented in this study is performed using radiosonde data from the IGRA archive and GPS data from the COSMIC/SuomiNet network (Section 2.2). Furthermore, GOME-2 results are compared with independent TCWV data from the ECMWF ERA-Interim reanalysis (Section 2.3) and with the Remote Sensing System (REMSS) SSMIS satellite F16 ocean product (Section 2.4) during the full period January 2007-March 2015.

On the basis of the validation results we are able to identify improvements required in the retrieval algorithm and to assess the quality of the satellite product (Threshold accuracy: 25%; Target accuracy: 10%; Optimal: 5%), as stated in the O3MSAF [PRD].

1.2   Preliminary remarks

The operational GOME-2/MetOp-A and GOME-2/MetOp-B TCWV products used in this study are developed in the framework of EUMETSAT's Satellite Application Facility on Ozone and Atmospheric Chemistry Monitoring (O3M-SAF) and generated by DLR using the UPAS environment version 1.3.9 and the level-1-to-2 GOME Data Processor (GDP) version 4.8.

The retrieval algorithm is based on a classical Differential Optical Absorption Spectroscopy (DOAS) method and combines a H_2O and O_2 retrieval for the computation of the trace gas vertical column density. In order to eliminate the dependency of the data set on the viewing angle conditions a distinct empirical correction is applied over land and ocean surfaces. The main improvement that has been made in the algorithm is a new computation of the cloud fraction and cloud top albedo measurements. The same cloud treatment has been consistently applied both to GOME-2/MetOp-A (GOME-2A) and to GOME-2/MetOp-B (GOME-2B) measurements. We analyze the accuracy of the GOME-2 satellite products through a detailed comparison of the two data sets. Ground-based measurements, simulated data sets and independent satellite observations are used to further document the geophysical consistency of the H_2O column data.

The validation and comparison studies were carried out at the Finnish Meteorological Institute (FMI) and at the German Aerospace Center, Remote Sensing Technology Institute (DLR-IMF).

1.3   Structure of the document

Section 2 gives an overview of the GOME-2/MetOp-A and GOME-2/MetOp-B product together with a description of the retrieval algorithm used for the retrieval of the H_2O column. We also introduce the data sources used for the validation with ground-based measuremnts and for the comparison with independent satellite products and model data. In Section 3 the GOME-2B water vapour columns are compared with those from its predecessor GOME-2A for the period December 2012 through March 2015. The results of the validation with radiosonde data from the Integrated Radiosonde Archive (IGRA) and GPS data from the COSMIC/SuomiNet network can be found in Section 4 (Kalakoski et al., 2014). Detailed comparisons between the GOME-2 water vapour columns from MetOp-A and MetOp-B and both the ECMWF ERA-Interim data and satellite measurements from SSMIS satellite F16 are illustrated in Sections 5 and 6, respectively. Finally, conclusions are drawn in Section 7.

2. DATA SOURCES

2.1 GOME-2 total column water vapour product

GOME-2 total column water vapour product is derived from measurements of the GOME-2 instruments aboard EUMETSAT polar-orbiting MetOp-A and B satellites. In this document we evaluate the GDP 4.8 total column water vapour product. Measurements are available over the period January 2007 to March 2015 for MetOp-A and from December 2012 to March 2013 for MetOp-B.

2.1.1 Retrieval Algorithm

The algorithm we use for the retrieval of the total column water vapour is based on a classical Differential Optical Absorption Spectroscopy (DOAS) performed in the wavelength interval 614-683 nm. It consists of three basic steps (described in details by Wagner et al., 2003, 2006).

In the first step, the spectral DOAS fitting is carried out, taking into account the cross sections of O_2 and O_4, in addition to that of water vapour. To improve the broadband filtering, 3 types of vegetation spectra are included in the fit, together with a synthetic Ring spectrum and, finally, an inverse solar spectrum to correct for possible offsets, e.g. caused by instrumental stray light. In the second step, the water vapour slant column density (SCD) is corrected for the non-linearities arising from the fact that the fine structure water vapour absorption lines are not spectrally resolved by the GOME instrument. In the last step, the water vapour SCD is divided by a "measured" Air Mass Factor (AMF) which is derived from the simultaneously retrieved O_2 and it is defined as the ratio between the measured SCD of O_2 and the known VCD of O_2 for a standard atmosphere. This simple approach has the advantage that it corrects in first order for the effect of varying albedo, aerosol load and cloud cover without the use of additional independent information. It is also important to remark that, in contrast to most other algorithms, our water vapour analysis from GOME-2 does not rely on additional information, except for the use of an albedo database (based on surface reflectivity data from Grzegorski 2009, and Koelemeijer et al., 2002) for the AMF correction. This serves the aim to derive a climatologically relevant time series of Total Column Water Vapour (TCWV) measurements (Wagner et al., 2006; Lang et al., 2007; Noël et al., 2008).

Compared to GOME-1 (Burrows et al., 1999) and SCIAMACHY (Bovensmann et al., 1999), the observations of GOME-2 have a much wider swath (1920 km scan width). While this broader swath results in a largely improved coverage, also some modification to the H_2O retrieval becomes necessary. In particular, we observe that water vapour total column present a significant Scan Angle Dependency (SAD). There is a bias up to 1 g/cm^2 between the H_2O product for the west and east part of the swath and the central ground pixels. The effect is particularly strong over ocean areas, while the land surface is less affected.

In GDP 4.8 we use the empirical correction for the scan angle dependency introduced in the previous version of the algorithm (GDP 4.7). The correction is based on the GOME-2A full time series and is computed separately over land and ocean surfaces, to take into account the diverse reflectivity properties of the surface. It is computed as follows. Multi-annual monthly mean H_2O total columns are created and employed to select the latitudinal binned regions which contains a sufficient large number of measurements to avoid that the correction is affected by natural variability in the H_2O total columns. Scan angle read-outs toward the nadir scan angle (scan pixel

numbers 9-10-11) are then used as reference values to normalize the H_2O total column for every forward angle position and derive a self-consistent correction. Finally, a polynomial is fitted to the normalized measurements in order to remove outliers and obtain a smooth correction function. With this procedure, residuals are of the order of few percent and the bias between the east and west part of the scan is reduced to negligible values.

The water vapour retrieval algorithm uses two cloud indicators to identify and flag cloudy pixels. This is necessary to remove potential systematic effects due to the different altitude profiles of H_2O and O_2 which might still appear in the water vapour product.

The first H_2O cloud flag is set if the retrieved O_2 slant column is below 80% of the maximum O_2 SCD for the respective solar zenith angle (roughly when about 20% from the column to ground is missing). Especially for low and medium high clouds, the relative fraction of the VCD from the ground which is shielded by clouds for O_2 and H_2O can be quite different. Therefore, we require that the main part of the O_2 column is present.

The second cloud flag is set if the product of cloud fraction and cloud top albedo exceeds 0.6 (anomalously high cloud top reflection). In this case, the H_2O total column is also set to "invalid" as the pixel might be considered fully clouded. The GOME-2 cloud fraction is determined with the OCRA algorithm using broadband radiance measurements in the UV/VIS range, while cloud-top height and cloud-top albedo are retrieved with the ROCINN algorithm using the spectral information in the Oxygen-A band in and around 760 nm (Loyola et al., 2007 and 2010).

In the new versions of the water vapour retrieval algorithm (GDP 4.8) the computation of the cloud properties has been reviewed: the cloud values are now also retrieved for ice and snow conditions and the shape of the cloud fraction distribution has changed (Lutz et al., 2015). The total number of observations rejected as cloudy is lower than with the GDP 4.7 retrieval algorithm, especially at high latitudes. Also the mean cloud top albedo values are slightly larger in the new data set (by about 15%), while the cloud fraction retrieved is reduced. Therefore the second cloud flag criteria (cloud fraction * cloud top albedo < 0.6) is fulfilled in a larger number of cases.
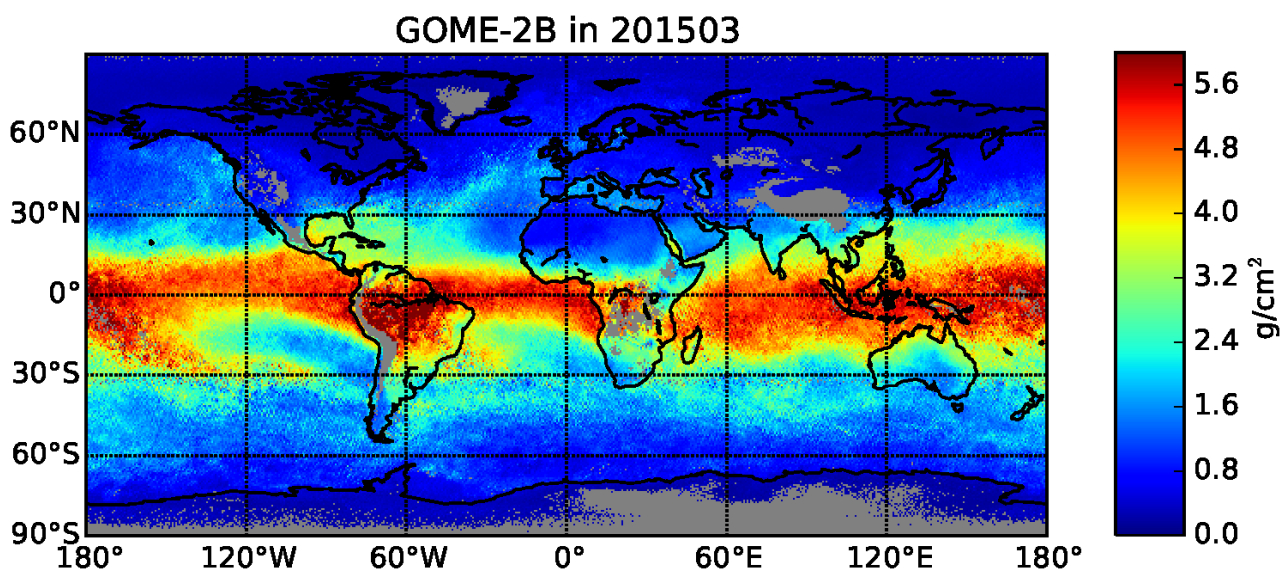
Figure 2.1: Monthly mean maps of total column water vapour from GOME-2B in March 2015.

Figure 2.1 shows the mean distribution of GOME-2B total column water vapour data in March 2015 for cloud-free conditions. In contrast to other satellite data sets, the GOME-2 product has the advantage that it covers the entire Earth, including both ocean and continents, leading to a more consistent picture of the global distribution of the atmospheric humidity. Moreover, the retrieval is performed in the visible/near-infrared spectral range and it is very sensitive to water vapour in the lower troposphere, which contributes the major fraction of the total atmospheric column.

2.2 Ground-based observations and co-locations

2.2.1 Radiosonde data

Water vapour column data used for comparisons was obtained from the Integrated Global Radiosonde Archive (IGRA). IGRA is a radiosonde dataset maintained by National Climatic Data Center (NCDC). IGRA contains quality-assured observations from 1500 globally distributed stations with different periods of record from 1960s to present. For the period of this validation, the data source is the NCDC real-time Global Telecommunication System (GTS) dataset. Quality assurance procedures are described in detail in Durre et. al (2006). In 2003, 74% (35%) of all soundings reached 100-hPa (10-hPa) level. Average sounding has 46 levels (vertical resolution 0.5 km).

2.2.2 GPS data

GPS observations were obtained from the COSMIC/SuomiNet network, a ground-based GPS network designed for real-time remote sensing of atmospheric water vapour. The network provides integrated atmospheric water vapour columns and the total electron content from globally distributed GPS stations. Precipitable water estimates are provided for each station at 30 min time resolution.

2.2.3 Co-location criteria

In all comparisons against ground-based observations, the GOME-2 measurements were screened for cloudy scenes using the cloud flag included in the product files. The measurements with solar zenith angle > 75º were discarded to exclude low light conditions. Only forward-scan pixels were used for comparisons, since back-scan pixels are of a larger size. GOME-2A observations are compared from the beginning of the data availability (January 2007 and 13 December 2012 for GOME-2A and GOME-2B, respectively) until March 2015 (radiosondes) and February 2014 (GPS). It should be noted, that the availability and spatial representativeness of the GPS observations degrades in the last months of the data record.

For our analysis of the radiosoundings, we selected the measurements where the stations are located within the GOME-2 ground pixel and the sounding times coincide within three hours of the Metop overpass. This means that the centres of GOME-2 pixels are within 50 km of the sonde launch sites in the majority of cases. The water vapour columns were calculated by integrating the specific humidity measurements from the surface up to the altitude of the lapse-rate tropopause, which is specified in the IGRA profiles. Soundings without an identified tropopause were discarded. Only profiles with more than 20 altitude levels were used for the analysis. After the screening, the total

number of co-locations with the radiosondes was about 580000 for GOME-2A and 159000 for GOME-2B.

Similarly, we use GPS measurements located within the GOME-2 ground pixels. Because of the better temporal resolution of the GPS measurements, only the observations with smallest available time difference to the MetOp overpass were selected for each coincidence. Since the GPS retrievals are available all day at a frequency of 30 minutes, only co-locations where the time difference between the GOME-2 overpass and the GPS retrieval was less than 15 minutes were used. Following a recommendation from the processing team, we have only used the GPS measurements that have a formal error of the precipitable water vapour (as specified in the data files) not exceeding 0.3 mm. The total number of co-locations with the GPS was about 123,000 for GOME-2A and 15,000 for GOME-2B.

Locations of the radiosonde and GPS co-locations for GOME-2A are shown in Figure 2.2. While radiosonde observations are widely available, co-location criteria mean that accepted co-locations are concentrated in two bands (South America to Europe and Western Pacific). Since GPS co-locations are available at smaller time intervals, no such concentration is seen there. However, number of stations and observations is much smaller.
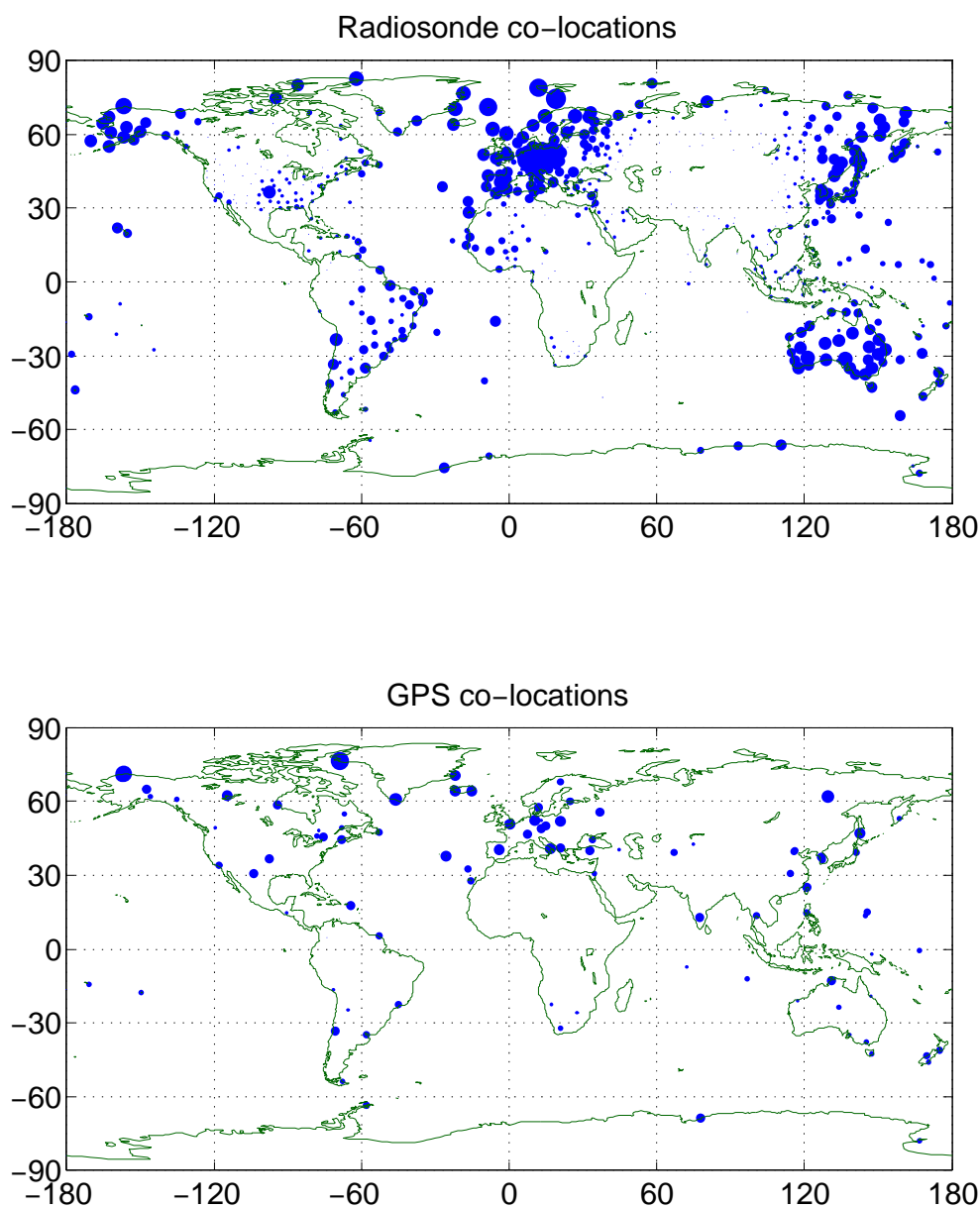
Figure 2.2: Locations of the GOME-2A co-locations against a radiosondes (top) and GPS (bottom) observations. Size of the markers is proportional to the number of co-locations.

2.3 ECMWF ERA-Interim data set

In this document GOME-2A and GOME-2B measurements are compared with corresponding data from the European Centre for Medium Range Weather Forecasts (ECMWF). The H_2O total column data are based on the ECMWF ERA-Interim reanalysis data set (Dee et al., 2011a; 2011b) between January 2007 and March 2015. For the comparison we combine the ECMWF ERA-Interim forecast

12 hour values produced from forecasts beginning at 00 and 12 Coordinated Universal Time (UTC) to derive a daily mean H_2O total column.

ERA-Interim is the latest global atmospheric reanalysis produced by ECMWF and provides a coherent record of the global atmospheric evolution constrained by the observations during the period of the reanalysis (1979 to present). An advantage of using reanalysis data for the comparison is that they provide a global view that encompasses essential climate variables in a physically consistent framework. The results are produced with a sequential data assimilation scheme, in which available observations are combined with prior information from forecast models, in order to estimate the evolving state of atmospheric water vapour. Gridded data products include a large variety of 3-hourly surface parameters, describing weather as well as ocean-wave and land-surface conditions, and 6-hourly upper-air parameters covering the troposphere and stratosphere. The accuracy of the data assimilation scheme, however, will depend on the quality and availability of observations in the selected time frame. Large errors in reanalysis products can originate from the lack of observations, changes in the observing system and shortcomings in the assimilation model.

The improved atmospheric model and assimilation system used in ERA-Interim reduces significantly several of the inaccuracies exhibited by the previous ERA-40 reanalysis, such as too-strong precipitation over oceans from the early 1990's onwards and a too-strong Brewer-Dobson circulation in the stratosphere. Known key limitations of the ECMWF ERA-Interim data set are a very intense water cycling (precipitation, evaporation) over the oceans and positive biases in temperature and humidity (below 850 hPA) compared to radiosondes in the Artic.

Figure 2.3 shows the distribution of the monthly mean TCWV product in March 2015 obtained combining ECMWF ERA-Interim daily forecasts at 0:00 and 12:00 UTC.
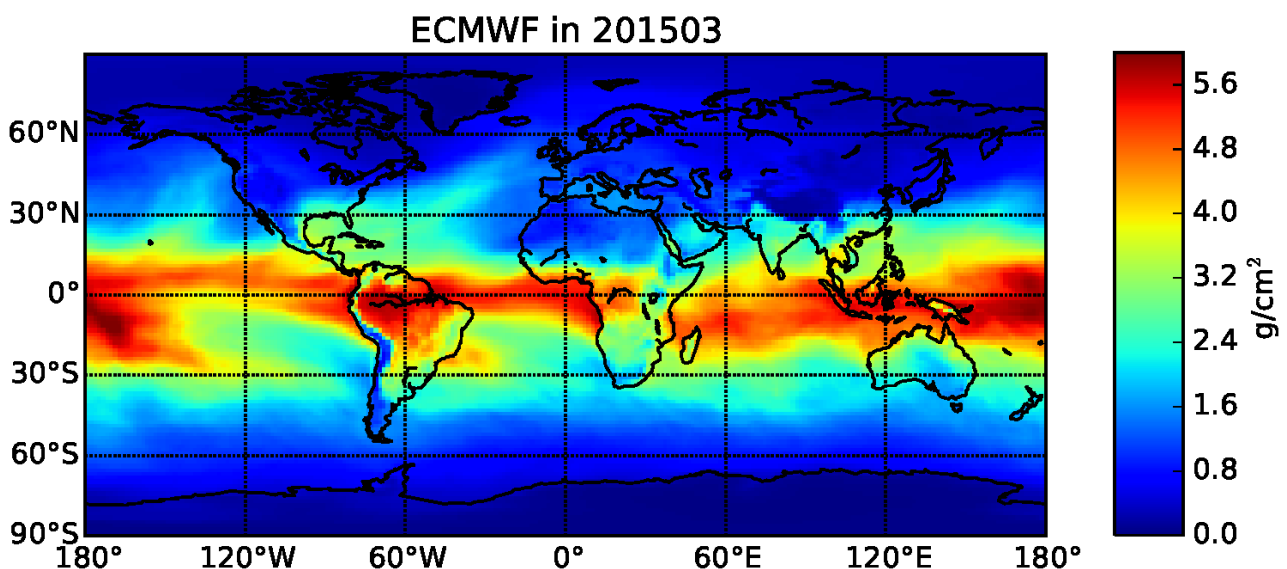
Figure 2.3: Geographical distribution of the mean H_2O vertical columns derived from the ECMWF ERA-Interim data set in March 2015.

2.4   SSMIS satellite F16 data set

For the validation of GOME-2 H_2O total column we used passive microwave observation from the Special Sensor Microwave Imager Sounder (SSMIS) orbits of the F16 satellite. These data are produced by the Remote Sensing System and sponsored by the NASA earth science MEaSUREs DISCOVER projects (REMSS, http://www.ssmi.com/ssmi). The series of 7 Special Sensor Microwave / Imager (SSM/I) have been in orbit since 1987 on various platforms, predominantly those of the Defense Meteorological Satellite Programs (DMSP) F-platforms, and now the SSM/I series has been replaced by a combined imager/sounder called SSMIS. In this study, we use SSMIS measurements of the F16 polar orbiting satellite between January 2007 and March 2015.

The SSMIS data products are generated using a unified algorithm to simultaneously retrieve ocean wind speed, atmospheric water vapor, cloud liquid water, and rain rate (Wentz, 1997). This algorithm is based on a physical model for the brightness temperature of the ocean and intervening atmosphere, and is the product of 20 years of refinements, improvements and verifications. Radiative transfer theory provides the relationship between the Earth's brightness temperature and the geophysical parameters (surface temperature, near-surface wind speed and vertically integrated cloud liquid water), which are used for the retrieval. TCWV data are available over ocean only and rely on independent calibration against radiosonde (Wentz, 2013). However, they also include TCWV for cloudy scenes, both day and night overpasses and span a very large time range. As an example, the mean total column water vapour distribution from SSMIS F16 for March 2015 is shown in Figure 2.4.
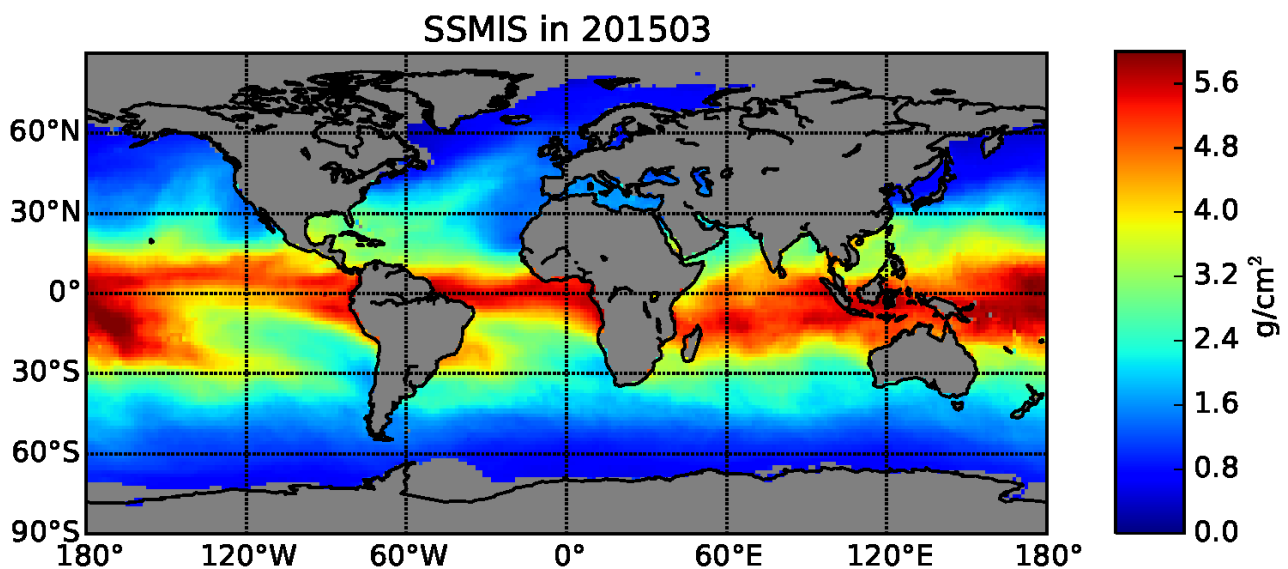
Figure 2.4: Geographical distribution of the mean H_2O vertical columns derived from SSMIS F16 measurements in March 2015.

3. EVALUATION OF THE H_2O COLUMN DATA PRODUCT

3.1   Comparison between GOME-2/MetOp-A and GOME-2/MetOp-B

We compare the GOME-2/MetOp-B H_2O VCDs with those from its predecessor GOME-2/MetOp-A in the overlap period from December 2012 to March 2015. We perform the inter-comparison between GOME-2A and GOME-2B data taking into account either (mostly) cloud-free or all available measurements for one particular day and monthly means. For the monthly comparison, we first analyze the spatial distribution of the bias from gridded monthly mean GOME-2A and GOME-2B water vapour columns. Then, in order to make the data selection in the two instruments as similar as possible, a comparison using only co-located measurements is performed. A quantitative analysis of the bias between GOME-2A and GOME-2B as a function of the latitude concludes this Chapter.

3.2   Daily GOME-2 comparison

Figure 3.1 shows a daily map of the H_2O columns for the 30th March 2013 from GOME-2A (left panel) and GOME-2B (right panel) measurements and provides a first illustration of the geophysical consistency of the total H_2O column products from the different instruments. Since the 15th July 2013 the GOME-2 satellites operate in a tandem mode. In the tandem mode the GOME-2A observations use a reduced swath of 960 km with a resolution of 40 x 40 km, while GOME-2B operates on the nominal wide swath of 1920 km (see Figure 3.1). This configuration allows us the use of the higher spatial resolution data to further study the consistency of the two products in the overlap regions of the GOME-2A and GOME-2B orbits.

Overall, we observe a very good agreement between the two data sets and the same spatial patterns in the humidity distribution, with high values in the tropics and low humidity at higher latitudes. Since the GOME-2 products are only derived from daylight observations, a large area around the Antarctic is blanked out. Here, we do not apply any cloud mask to the data to show the daily coverage of the two GOME-2 instruments, which follow co-planar orbits, 174° out of phase.
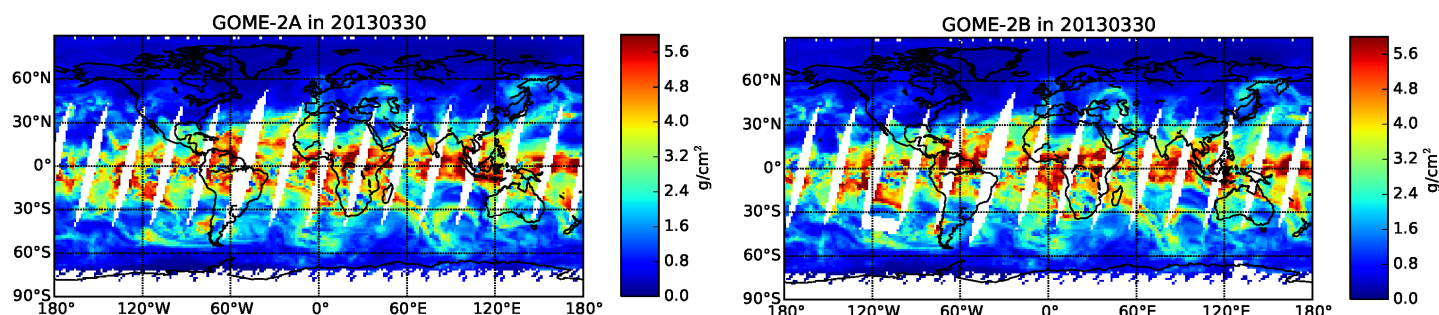
Figure 3.1: Daily averages of total H_2O vertical columns from GOME-2A (left panel) and GOME-2B (right panel) for the 30th March 2013. All measurements are shown (no cloud flagging).

In Figure 3.2 we investigate the dependence of the differences between GOME-2A and GOME-2B water vapour co-located measuements for the 30th March 2013 with (top panel) and without (bottom

panel) cloud flagging. Co-location areas are determined selecting all measurements within a pixel size of 1.5 x 1.5 degrees in a given day. In the tropics the number of measurements is drastically reduced not just because of the larger chance of clouds, but principally because we have the least overlap there between the GOME-2A and GOME-2B orbits. In fact, the GOME-2A and GOME-2B co-planar orbits are 174° out of phase. This results in a temporal separation of the measurements at co-locations of approximately 48 minutes, and leads to differences in the TCWV because of tropospheric dynamics.

On average the H_2O VCD for GOME-2B is slightly higher than for GOME-2A product (see Table 3.1), with mean bias values between -0.045 and -0.035 g/cm^2 depending on whether we compare measurments with or without cloud masking. However, the median bias has lower values and does not change significantly in the two comparisons. In the cloud-free case, only 15% of the measurments have bias less than 0.1 g/cm^2. In the top panels of Figure 3.2 we can observe extended regions with bias very closed to 0 (white regions) not just at high latitudes, but also in the sub-tropical regions, like continental Northern Africa and Asia. Remaining differences in the tropics are mainly related to the presence of low clouds, the asymmetric cloud screening and low statistics (because of the smaller overlap regions).

Table 3.1: Statistics of the GOME-2A - GOME-2B comparison for the 30 March 2015, for measurements with and without cloud mask. Offset and slope refer to an orthogonal regression analysis.

GOME-2A – GOME-2B (30.03.2013)	Bias (mean) (g/cm^2)	Bias (median) (g/cm^2)	RMSE (g/cm^2)	Slope (-)
With cloud mask	-0.0442	-0.02147	0.315	0.9554
Without cloud mask	-0.0352	-0.02181	0.375	0.9618

3.3   Monthly GOME-2 comparison

The monthly mean product for the exemplary month March 2015 and for the GOME-2A and GOME-2B data sets is shown in Figure 3.3. The grid cells used to bin the GOME-2 measurements have an extent of 0.5^O latitude x 0.5^O longitude. Overall, we find very similar spatial patterns in the H_2O distribution. In Figure 3.4 we can observe the differences between GOME-2A and GOME-2B H_2O column. The mean global bias is small and negative (-0.045 g/cm^2). GOME-2B tends to produce slightly larger values than GOME-2A, but not more than 1.25%. The red and blue parts in the maps correspond to geographical locations with higher discrepancies. Over the continents and at high latitudes, the agreement between both data sets is generally very good. As discussed in the daily comparison, extended regions with very small biases are evident especially in Africa and Asia. Larger differences at low latitudes and over oceans are mainly due to the small number of co-located cloud-screened measurements. This effect is especially evident in some specific regions like the Western Pacific Warm Pool, South Africa and South America, where we have low statistics and uncertainties in cloud detections. Less than 9 % of the locations present a mean bias bigger than 0.5 g/cm^2 in absolute value and the mean difference between GOME-2A and GOME-2B H_2O VCDs is within the Product Requirements Document (PRD) optimal accuracy threshold. This shows that the GOME-2B H_2O total column product can be used for scientific purposes and to extend the GOME-type H_2O time series.
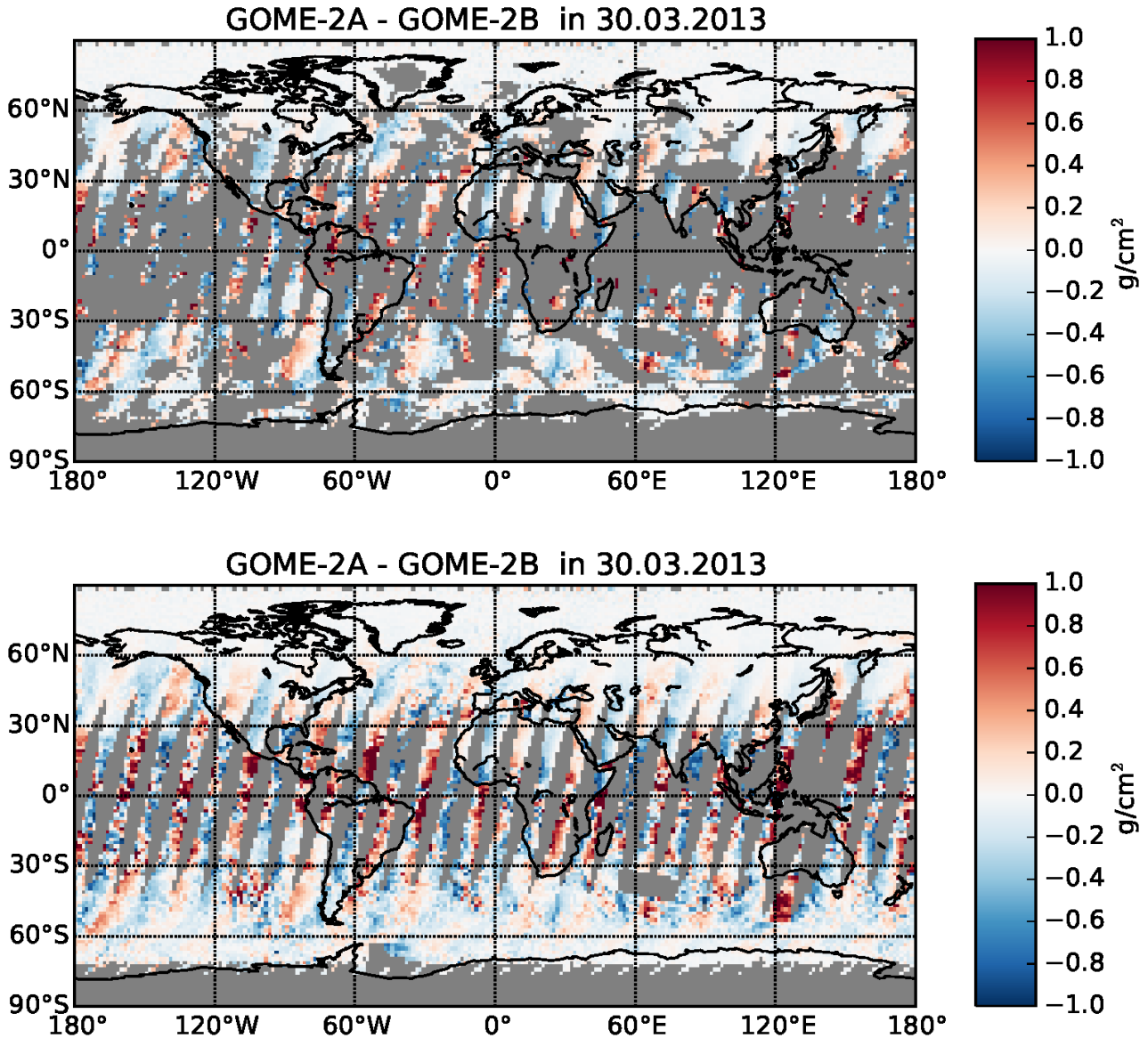
Figure 3.2: Geographical distribution of the differences between GOME-2A and GOME-2B water vapour column for the 30th March 2013 for cloud-free co-located measurements (top panel) and for all measurements (bottom panel).
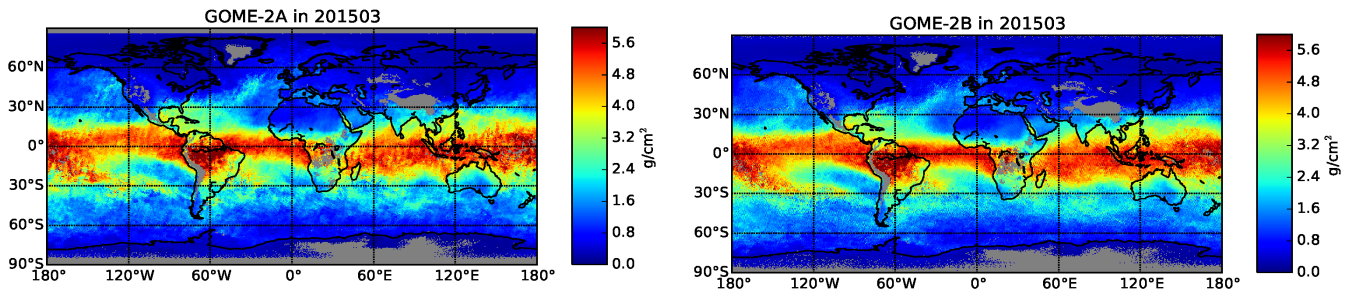
Figure 3.3: Monthly mean maps of total column water vapour from GOME-2A (on the left) and GOME-2B (on the right) for March 2015. Only cloud-screened data have been used.

		REFERENCE:	**SAF/O3M/DLR/ORR/H2O**
		ISSUE:	10/2015
		DATE:	30 October 2015
		PAGES:	18

EUMETSAT   O3M SAF
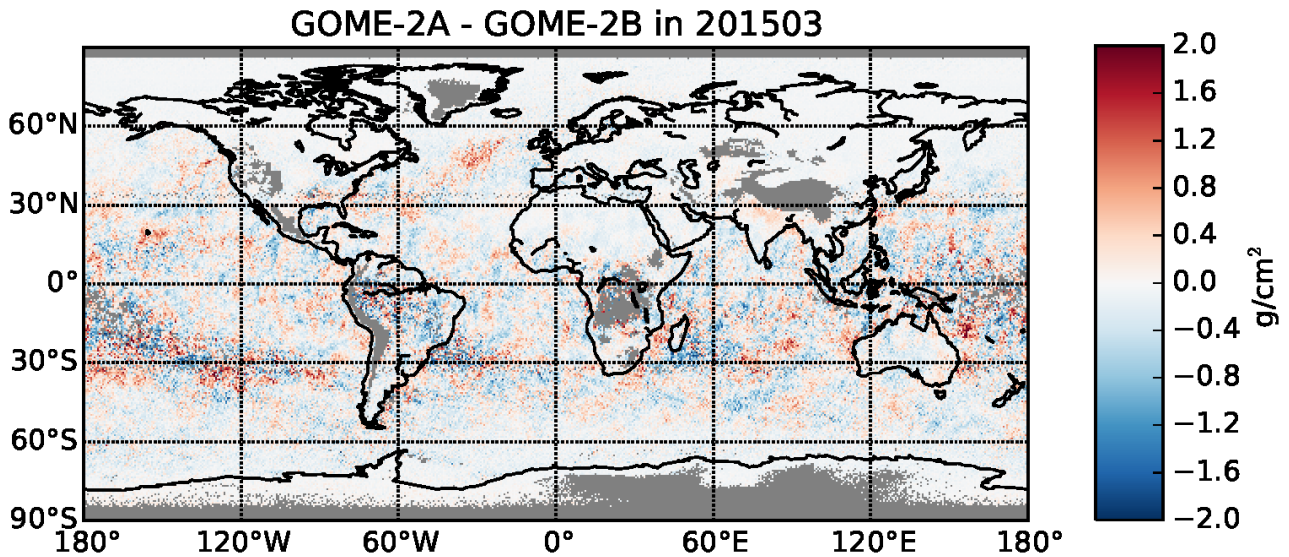
Figure 3.4: Geographical distribution of the differences between GOME-2A and GOME-2B water vapour column in March 2015. Only cloud-screened data have been used.

To access the consistency between the two data sets samples we also performed an orthogonal regression using the monthly mean data in each grid cell of the maps. Figure 3.5 shows the scatter plot of cloud-screened GOME-2A data against GOME-2B for March 2015 together with the histogram of the distribution of the differences GOME-2A – GOME-2B. The slope of the regression is very close to unity (0.97, offset 0.011 g/cm^2), consistently with the mean bias results.
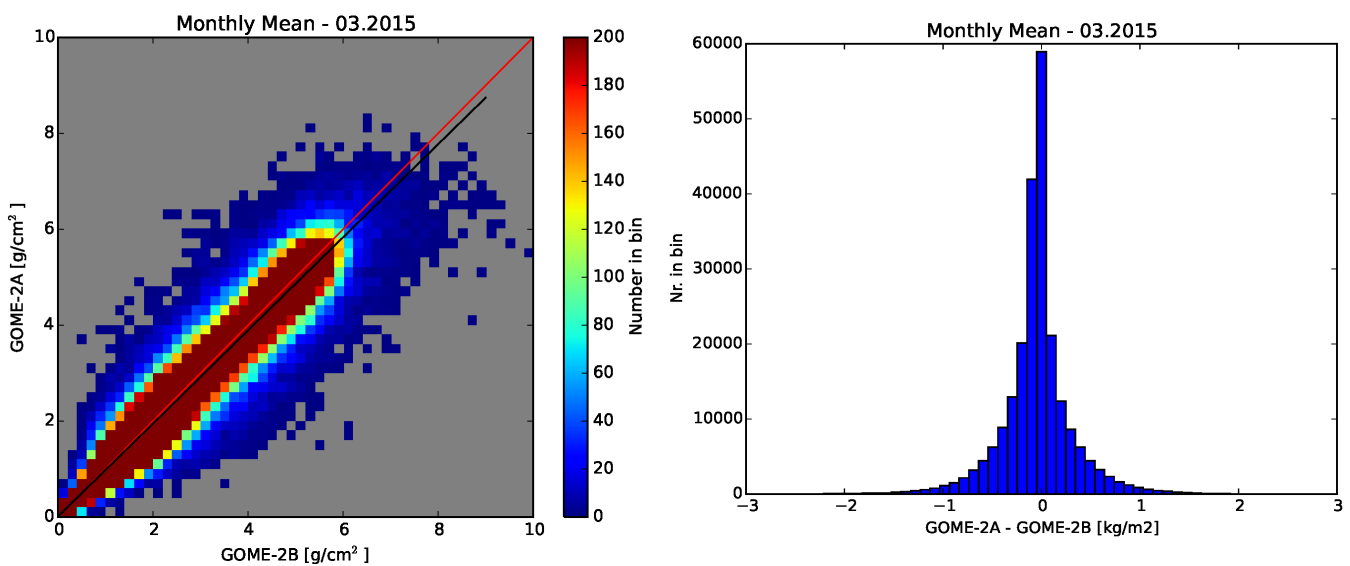
Figure 3.5: Left panel: scatter plot of GOME-2A monthly mean total columns against GOME-2B monthly mean total columns, for March 2015. Only cloud-screened data have been used.. Right panel: histogram of the difference GOME-2A - GOME-2B, for the points in the scatter plot.

In Figure 3.6 we show the global average bias between GOME-2A and GOME-2B for the period January 2013 to March 2015. The mean bias (red line) is computed comparing gridded monthly mean data. Averaging over the full time period, we find a small mean negative bias of -0.037 ± 0.009 g/cm^2 , while the biggest discrepancies are observed in January 2013 (mean bias of -0.053 g/cm^2). GOME-2B tends to produce slightly larger H$_2$O total column values than GOME-2A, but not more than 1.25%. The standard deviation for water vapour data is dominated by natural variability and therefore is quite large (see error bars in Figure 3.6).

We further investigate whether the East-West correction applied to both GOME-2 instruments (but calibrated only on GOME-2A data) might explain part of the differences in the water vapour content. The SAD correction strongly reduces the bias we would observe between the GOME-2A and GOME-2B after July 2013 due to the difference in swath width, however it doesn't introduce a shift between the data. We also verified that the ratio between the more extreme pixels in the swath (East/West scan numbers) is very close for both instrument and that the bias is present also when we compare separately the co-located eastern (or western) pixel scan numbers.

Very similar results are obtained using only co-located data, since the GOME-2A and GOME-2B data sets are processed with the same algorithm and the same cloud screening criteria. Figure 3.7 shows the distribution of the daily bias computed from co-located and cloud-screened measurments. In the box plot the central values (magenta) represents the median, the edges of the boxes the 25th and 75th precentiles and the wiskers are plotted at 1.5 times the likely change of variations (IQR). Points above or below this quantity are marked as outliers. Overplotted are also the mean values of the bias obtained from daily co-locations (green dashed line). The median values are very close to -0.05 g/cm^2 and the all data set range between 0 and 0.1 g/cm^2, including the outliers. The distribution of the data is rather symmetric with a small interquantile range (always less than 0.02 g/cm^2). The mean bias is slightly larger than the one obtained taking into account the monthly data distribution, because of the reduced amount of data. We can also observe a statistically significant decreasing trend in the bias between the GOME-2A and the GOME-2B measurments (null hypothesis is rejected at a 0.05 significant level). The evolution in the bias values however is present only in the daily co-located data (as opposed to the monthly co-locations, see Figure 3.6) and therefore is an effect of selection.
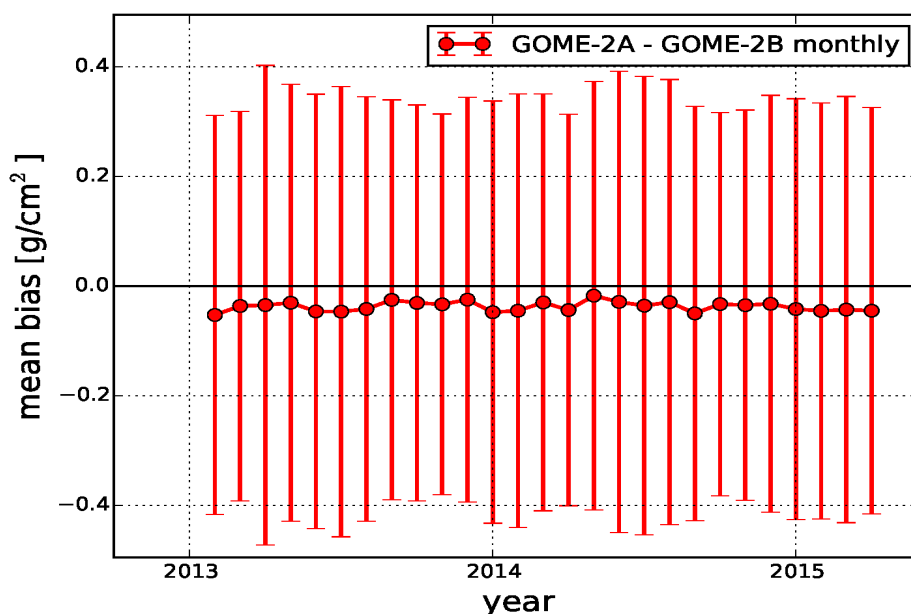
Figure 3.6: Global mean H_2O total column bias between GOME-2/MetOp-A and GOME-2/MetOp-B gridded monthly measurements for the period January 2013 - March 2015. The large error bars represent the standard deviation of the bias and are dominated by natural variability.
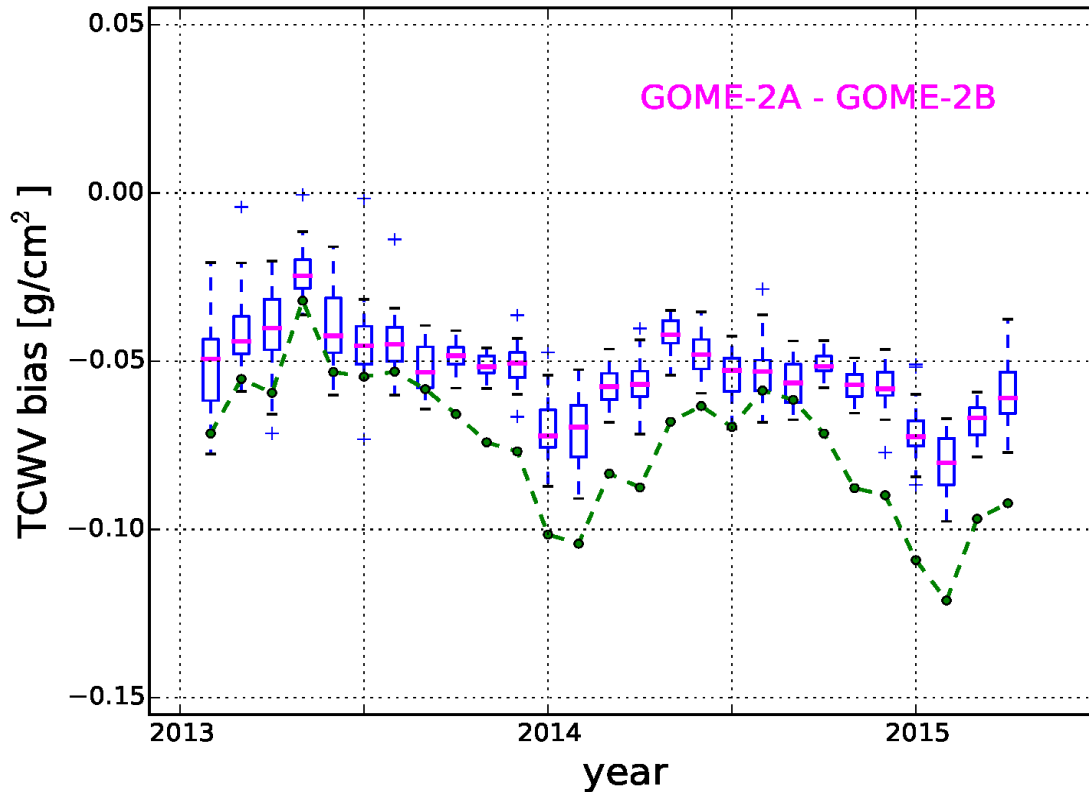
Figure 3.7: Global monthly median (magenta lines) and mean (green line) bias between GOME-2A and GOME-2B TCWV product.

3.4 Zonally averaged GOME-2 comparison

In this Section we investigate the differences between the GOME-2A and GOME-2B as a function of latitude and season. We compute the zonal average for 2.5$^{\mathrm{o}}$ latitude intervals and for cloud-free measurements only.

Figure 3.8 shows zonal TCWV values in July 2014, while in Figure 3.9 the comparison is performed for January 2015. The lines in the left panels of each plot represent the individual mean water vapour measurements as a function of latitude (red for GOME-2A, green for GOME-2B). From this plots we can infer that there is an excellent agreement between GOME-2A and GOME-2B measurements in both seasons and at all latitudes.

In order to examine more clearly the latitudinal variations, in the right panels of each plot (Figures 3.8 and 3.9) we show the difference GOME-2B - GOME-2A H_2O total column. On average, the GOME-2B total columns are slightly larger than the GOME-2A columns (about 2-3 % larger in relative value), which means that the GOME-2B data present a small wet bias with respect to GOME-2A. In July 2014 the bias ranges between +/-0.08 g/cm^2 and the mean bias is higher in the southern hemisphere than in the northern one. In Junuary 2015, on the other hand, we observe a bias

as large as -0.14 g/cm^2 at northern latitudes (+11.25 degree). However, the scatter is always within the error associated to the GOME-2 measurements.
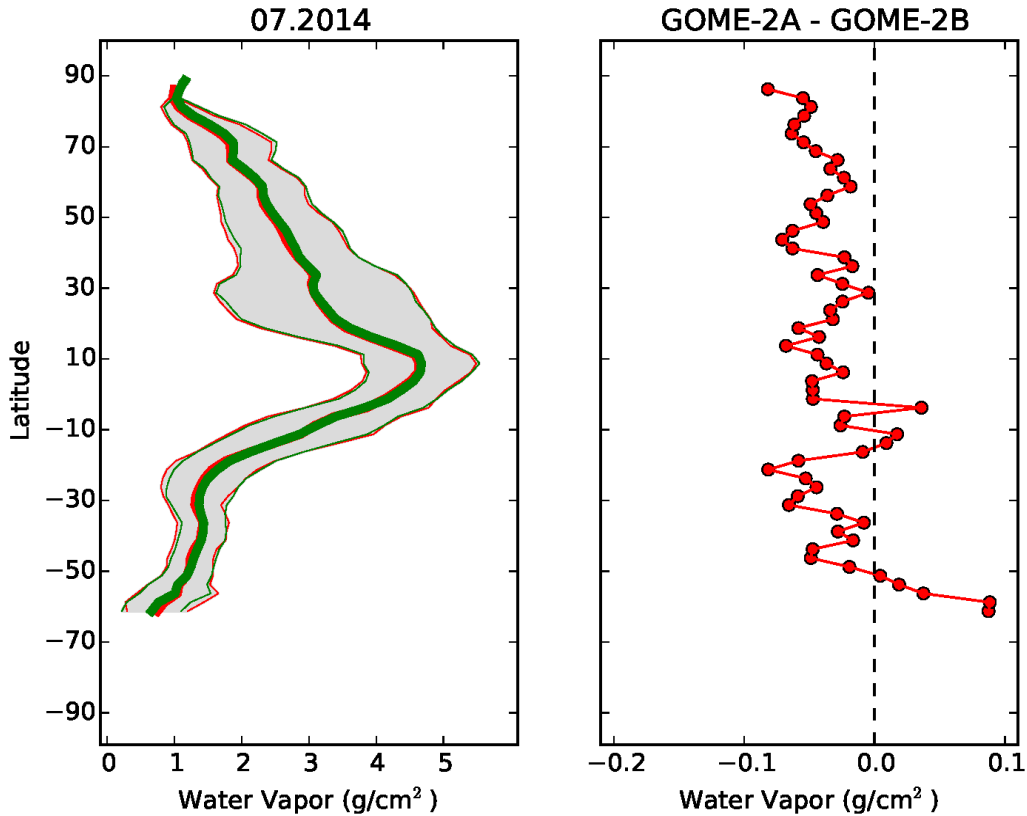
Figure 3.8: Zonal mean H_2O total column from GOME-2A (green points) and from GOME-2B (red points) as a function of latitude for July 2014 (left panel) and bias between GOME-2B and GOME-2A monthly averaged H_2O column (right panel). The results refer to cloud-free measurements. The shaded areas around the solid lines indicate one standard deviation.
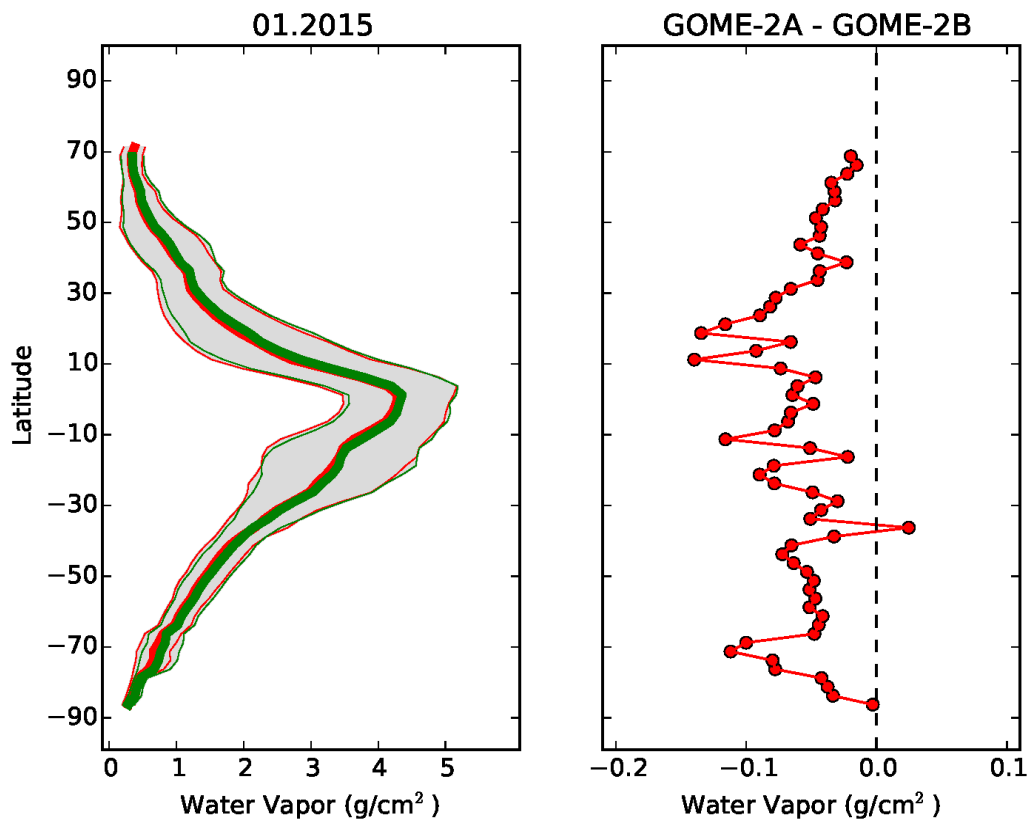
Figure 3.9: Same as Figure 3.8, but for January 2015.

4. COMPARISON WITH RADIOSONDES AND GPS

4.1   General comparisons

Comparisons against both radio sondes and GPS observations show generally good agreement for water vapour columns below 5 g/cm2 (See Figure 4.1). For larger water vapour amounts, GOME-2 underestimates the total column. For very low water vapour amounts, small overestimation is observed. Statistics of the comparisons are shown in Table 1. GOME-2A shows small dry bias against radio soundings, while for GOME-2B no such bias is observed. Both show similar wet bias against the GPS observations.

Time series of the global monthly median differences (Figure 4.2), shows small seasonal cycle in the bias and range of the differences. However, no statistically significant trend over full GOME-2A period could be found. Seasonal variation, especially in mid-latitudes, can be seen in figure 3, that shows the monthly median zonal relative difference in 10 degree latitude bands. Also visible in the figure is the difference between northern and southern hemispheres seen in the comparison with the radio sonde observations. Southern hemisphere mid latitudes show large positive biases, especially southern winter season, while northern hemisphere generally shows negative bias. The difference is probably related to difference difference in distribution of sea/land pixels, as well difference in local times of the co-locations.

Figure 4.4 shows the relative difference against radio sondes as a function of Solar zenith angle, cloud fraction and surface albedo. Dependency on SZA and albedo is fairly small, 5% difference in median between extremes. Larger differences are seen against cloud fraction, where the cases with nearly clear skies show positive bias, while cases with cloud fractions between 0.2 and 0.9 show negative biases. Fully cloudy cases again show positive biases.

Table 4.1: Statistics of comparisons between GOME-2A and B with radiosondes and GPS observations.

	Correlation coefficient	Mean difference [g/cm^2]	Mean relative difference	Standard deviation [g/cm^2]	Median difference [g/cm^2]	Median relative difference
GOME-2A - Sonde	0.915	-0.054	-0.6 %	0.518	-0.040	-3.7%
GOME-2A – GPS	0.935	0.049	13.7%	0.455	0.030	3.2%
GOME-2B - Sonde	0.915	0.002	8.0%	0.543	0.004	0.4%
GOME-2A - Sonde	0.942	0.042	16.6%	0.460	0.035	3.7%
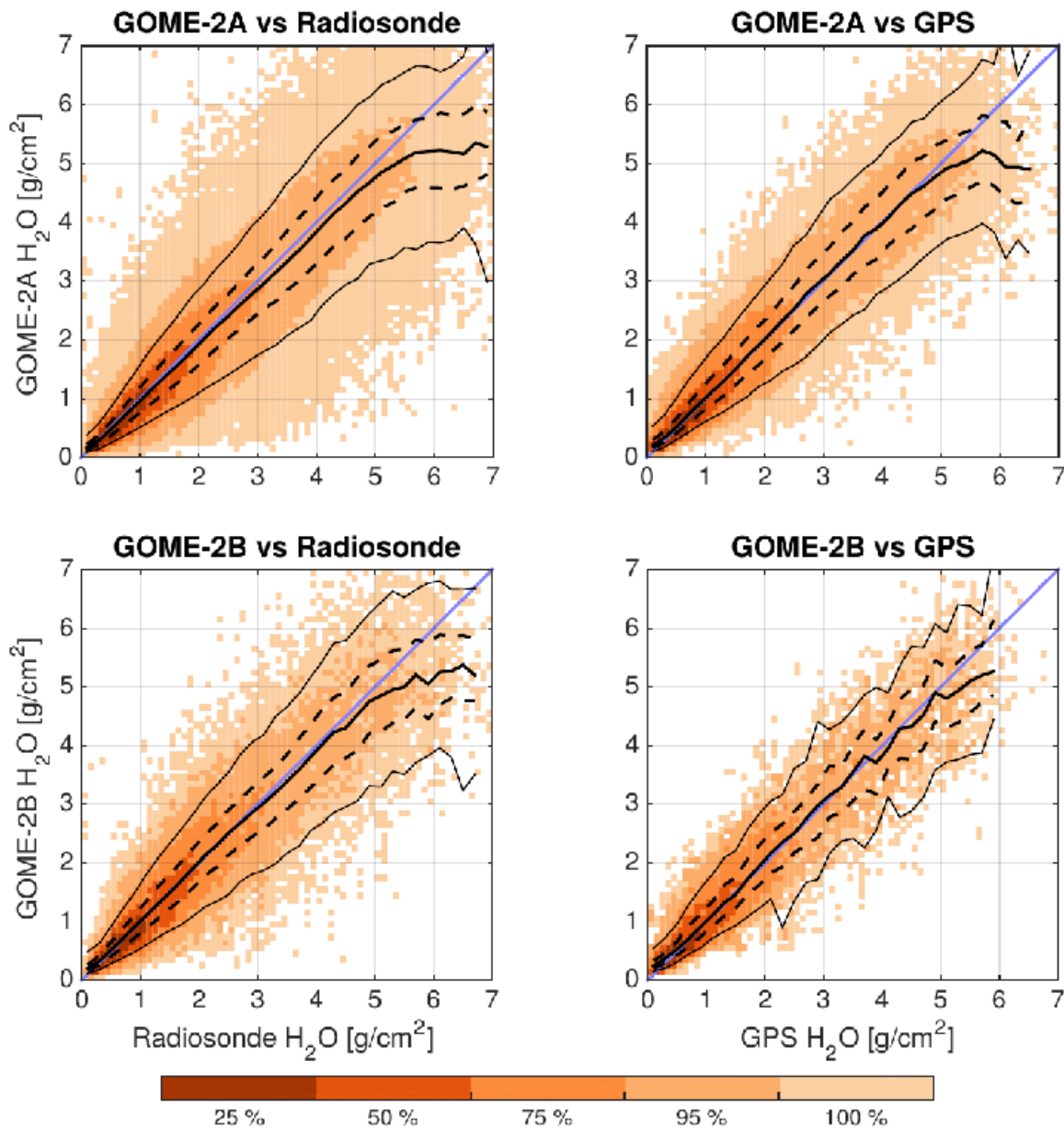
Figure 4.1: Scatter plot of GOME-2A (top) and GOME-2B (bottom) total water vapour columns against the IGRA integrated total water vapour columns (left) and COSMIC/SuomiNet GPS water vapour (right). Areas with darkest background color include 25% of all co-locations, while two, three, four and five darkest colors together include 50%, 75%, 95% and 100% of the co-locations, respectively. Solid line is the median of the GOME-2 water vapour column in 0.2 g/cm2 bin, dashed lines 25 and 75% percentiles and thin solid lines 5 and 95% percentiles. Solid blue line is x=y line.
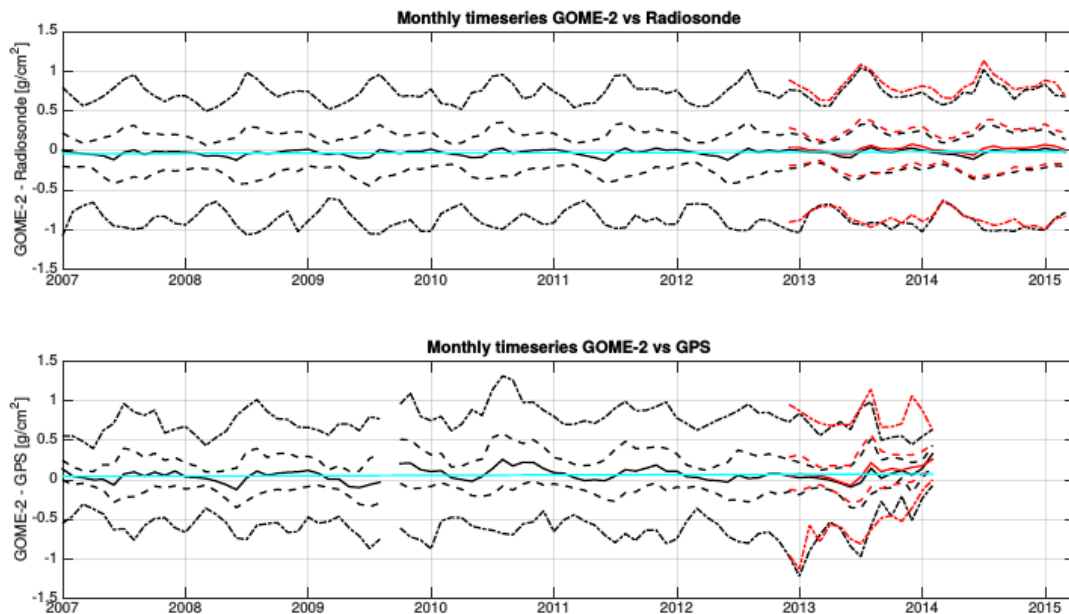
Figure 4.2: Time series of global monthly median differences (solid line), 25 and 75% percentiles (dashed lines) and 5 and 95% percentiles (dash-dot lines) for GOME-2A (black) and GOME-2B (red) against radiosonde (top) and GPS (bottom). Blue line shows the trend of the GOME-2A monthly medians (not significant).
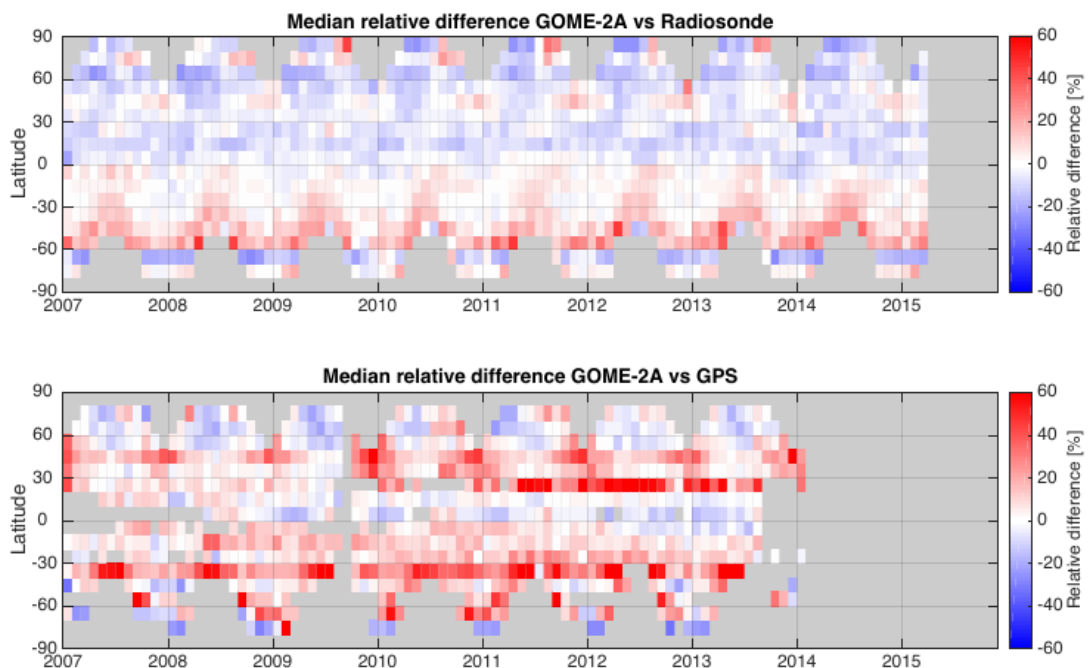
Figure 4.3: Monthly median relative difference [%] as a function of time and latitude, GOME-2A vs. radiosonde (top) and GPS (bottom). Each coloured box shows the median relative difference for one month in 10º latitude zone. Month-latitude bins with less than 10 co-locations are not shown.
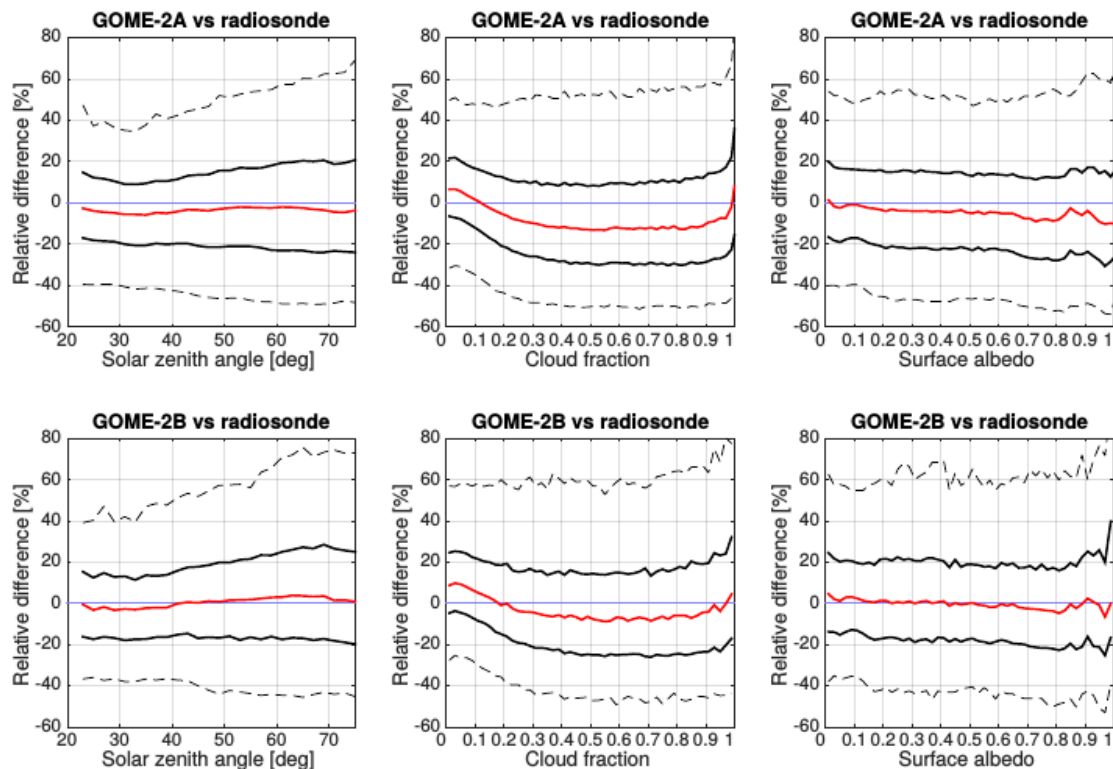
Figure 4.4: Median relative differences (red solid line), 25 and 75% percentiles (black solid lines) and 5 and 95% percentiles (dashed lines) for GOME-2A (top) and GOME-2B (bottom) against radiosonde as a function of solar zenith angle (left), geometric cloud fraction (center) and surface albedo (right).

4.2   Example comparisons

As an example of data, time series of GOME-2 and radiosonde observations for selected stations are shown in figures 4.5, 4.6 and 4.7. Stations chosen are the ones with largest number of co-locations in northern (Figure 4.5) and southern (Figure 4.7) mid-latitudes and in tropics (Figure 4.6). In general, GOME-2 and radiosonde observations match each other well, although in some cases very large differences are seen. In northern hemisphere, seasonal variation is seen in differences, but this is not as clear in relative differences. In tropics dry bias is observed in second half of the year, especially in August and September.

Difference in temporal coverage seen between northern and southern mid-latitudes stations is due to the difference in local time of the co-locations (see Fig. 4.8). Since the routine radiosonde launches are generally at set UTC times (0000 UTC and 1200 UTC), the local time of the launch, and therefore the co-location with GOME-2 observation, depends on the longitude of the station. In the case of southern hemisphere station shown in Figure 4.7, the morning sonde is launched in darkness for larger part of the year than in the case of the northern hemisphere station in Figure 4.5.
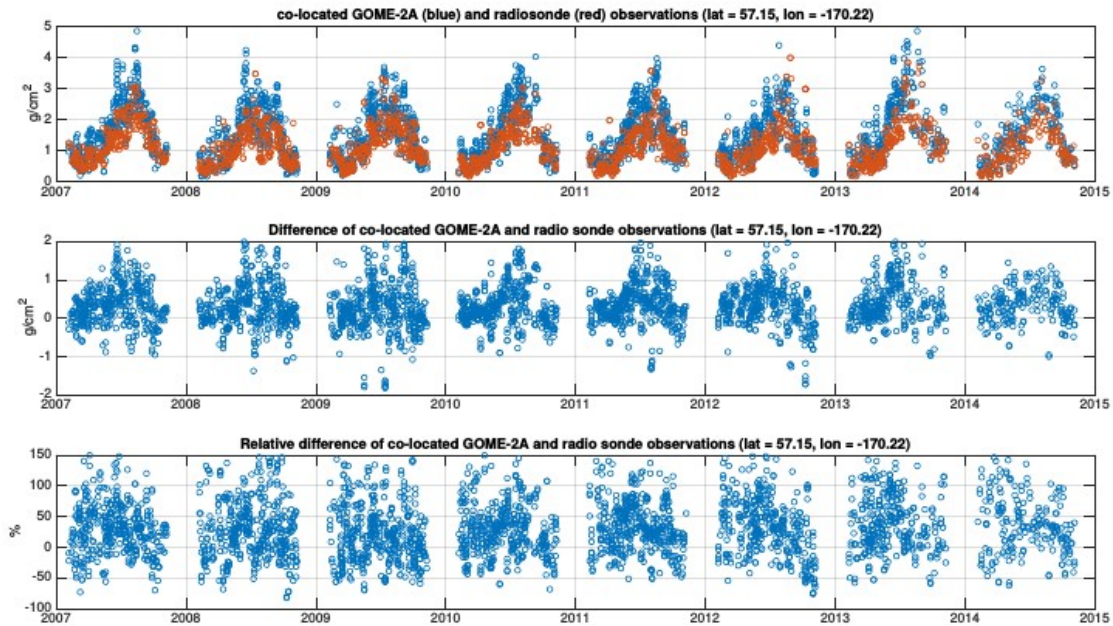
Figure 4.5: Comparisons with single stations in northern mid-latitudes: Top: Time series of GOME-2A (blue) and radiosonde (red). middle: Time series of difference GOME-2A - sonde. bottom: Time series of relative difference (GOME-2A – sonde)/sonde.
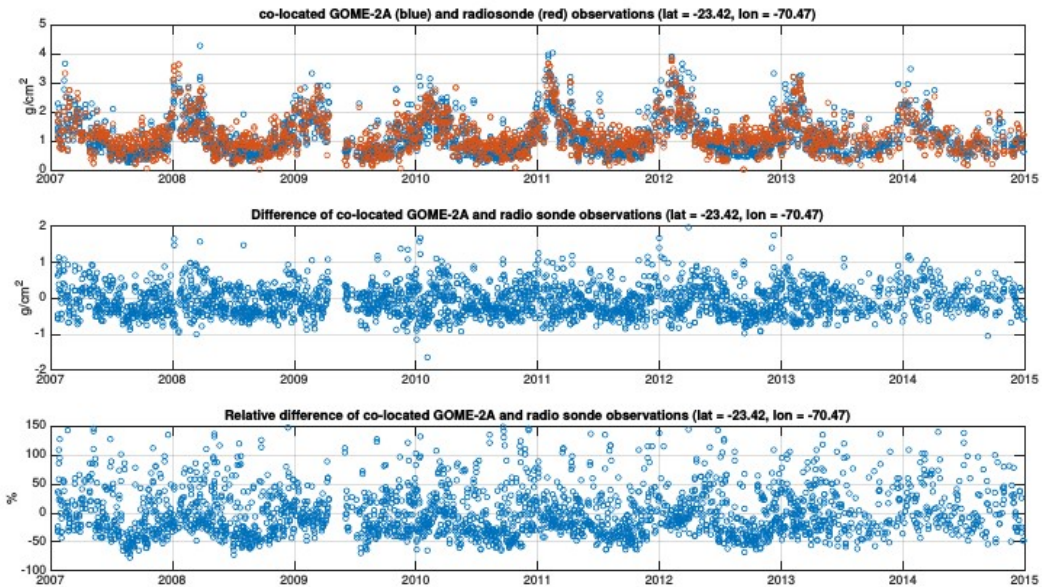
Figure 4.6: Comparisons with single stations in tropics: Top: Time series of GOME-2A (blue) and radiosonde (red). middle: Time series of difference GOME-2A - sonde. bottom: Time series of relative difference (GOME-2A -sonde)/sonde.
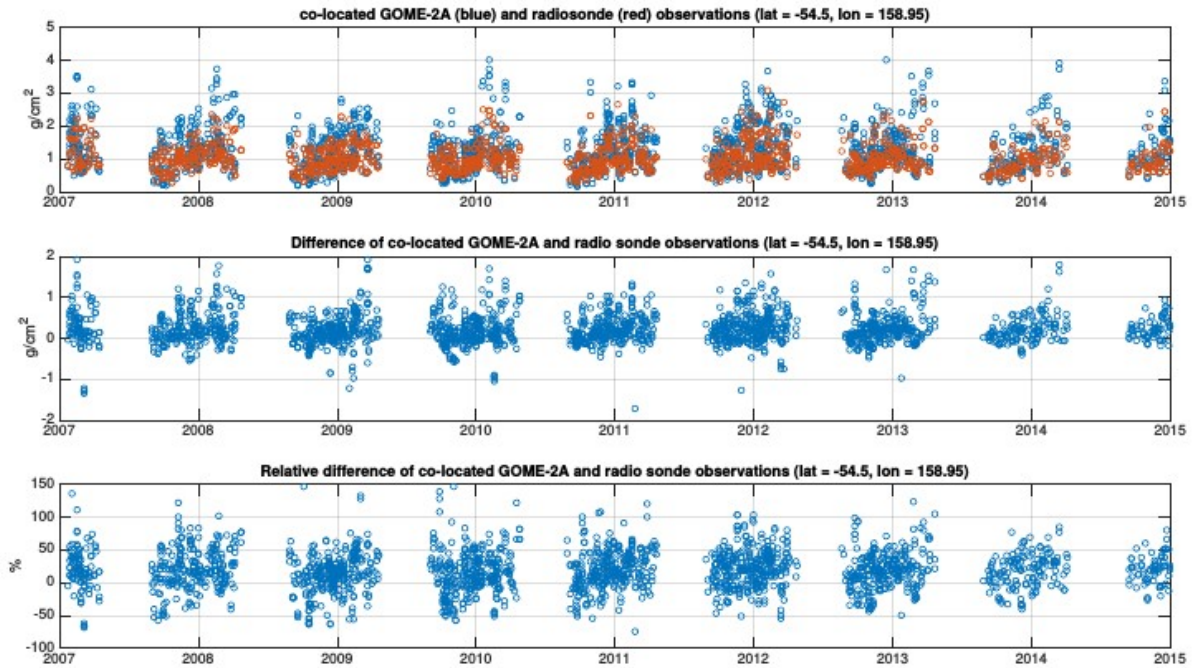
Figure 4.7: Comparisons with single stations in southern mid-latitudes: Top: Time series of GOME-2A (blue) and radiosonde (red). middle: Time series of difference GOME-2A - sonde. bottom: Time series of relative difference (GOME-2A – sonde)/sonde.
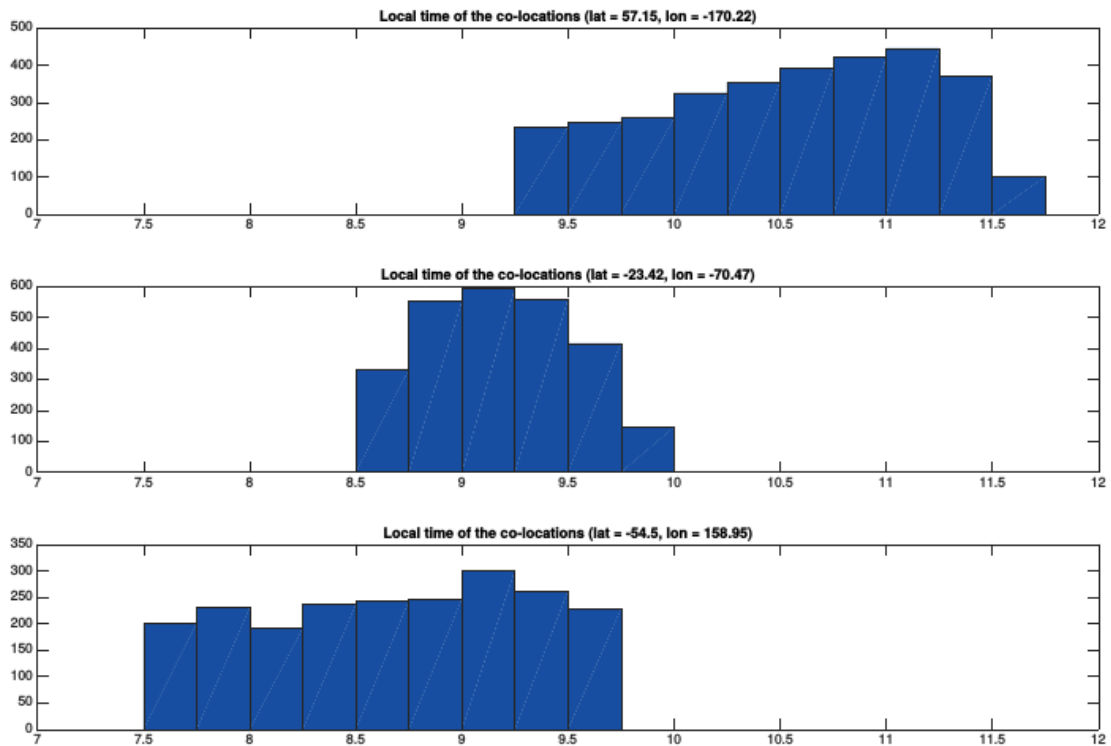
Figure 4.8: Histograms of approximate local times of the co-locations for the example stations.

5. COMPARISON WITH ERA-INTERIM TCWV

5.1   Method

For the comparison we use daily ECMWF ERA-Interim data obtained combining the forecast 12 hour values to derive a daily mean H_2O total column. We used the forecast data instead of the analysis data in order to have a more independent data set, since they include mostly modeling. In more detail, daily water vapour measurements are first gridded on a regular 1.5^O x 1.5^O spatial grid. Then, daily co-located data are used to compute the monthly mean bias between GOME-2 TCWV products and the ECMWF ERA-Interim data sets for the all period January 2007 - March 2015 (GOME-2A) and January 2013 – March 2015 (GOME-2B). The comparisons are performed for GOME-2 H_2O total columns which are not flagged as cloud-contaminated on the Level 2 data product. Pixels flagged as cloudy are removed on a daily basis also from the data sets selected for the comparison.

5.2   Global comparison

Figure 5.1 shows a time series of globally averaged mean bias of the TCWV distribution between GOME-2A and the ECMWF ERA-Interim data sets for the time period January 2007 - March 2015. Since January 2013 we have computed also the bias between the most recent GOME-2B results and a combined GOME-2 data set obtained by merging the observations from the MetOp-A and MetOp-B satellites.

The agreement between GOME-2 TCWV and ERA-Interim data is good for all comparisons: the mean biases for the full time series ranges between 0.034 g/cm^2 (for GOME-2A) and 0.086 g/cm^2 (for GOME-2B), while intermediate values are obtained for the combined GOME-2 data set. The small positive bias implies on average larger TCWV column in the GOME-2 data. On the other hand, the Root Mean Square Error (RMSE) is larger, about 0.3 g/cm^2 in all comparisons, as shown in Table 5.1. The RMSE for the water vapour measurements is evaluated from the mean squared difference between the GOME-2 sensor and the data set used for the comparison in each grid point. Because these deviations are squared before they are averaged, the RMSE gives a relatively high weight to large deviations. This means that the RMSE for the water vapour measurements is relatively high due to the high water vapour natural variations. The uncertainty margins provided for the bias and the RMSE statistics result from the spread of the bias and RMSE values in the time series. Since the GOME-2B total column data are typically larger than the GOME-2A data (see Chapter 3), also the bias is shifted towards higher values in this case.

Table 5.1: Bias and RMSE statistics. The computations refer to the average difference GOME-2- ECMWF ERA-Interim data. The time period analyzed is January 2007 – March 2015 for the comparison GOME-2A - ECMWF ERA-Interim, and January 2013 - March 2015 for the GOME-2B and GOME-2 (combined GOME-A and GOME-2B data) comparisons.

Data	Bias (g/cm^2)	RMSE (g/cm^2)
GOME-2A - ECMWF (01.2007-03.2015)	0.034 +/- 0.015	0.304 +/- 0.053
GOME-2B - ECMWF (01.2013-03.2015)	0.086 +/- 0.009	0.313 +/- 0.054

GOME-2 - ECMWF (01.2012-03.2015)	0.067 +/- 0.014	0.294 +/- 0.057
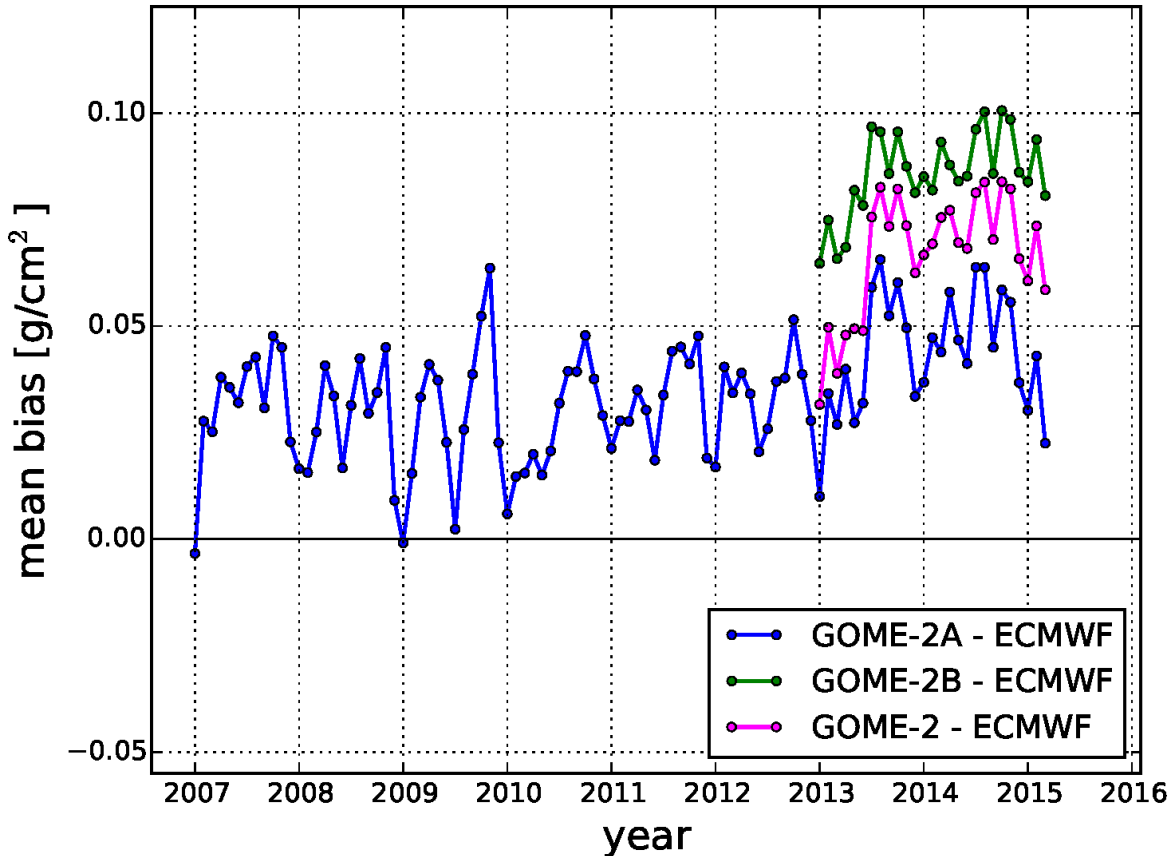
Figure 5.1: Global monthly mean bias between ECMWF ERA-Interim model data and GOME-2A TCWV (blue points), GOME-2B TCWV(green points) and combined GOME-2A and GOME-2B TCWV product (magenta points).

Figure 5.2 shows a box-plot created by averaging for each month the daily global bias between the combined GOME-2 product and the ECMWF ERA-Interim model data. The median distribution of the monthly bias (magenta lines) is always lower than the mean values visible in Figure 5.1, and it ranges between 0.018 and 0.063 g/cm^2 (January 2013 and August 2014, respectively). It is possible to recognize only small season oscillation around the median bias because of the compensating effect of having both land (negative bias in the northern hemisphere summer months) and ocean retrievals (positive bias in the northern hemisphere summer months). The amplitude of the winter-summer oscillations is 0.045 g/cm^2 at most. The median bias values averaged over the all time series is slightly positive (0.047 g/cm2) and very close to the mean results.

The spread in the data is generally higher in the summer months (exception is December 2014), but the difference between the upper and lower quartile remains relatively small (less than 0.038 g/cm^2). Finally, we observe both positive and negative outliers in a smaller fraction of the months (blue crosses in the plot).

In order to interpret these results and to assess the observed biases and seasonal cycle, in the next section we show the global distribution of the bias between ECMWF ERA-Interim model data and the GOME-2A and GOME-2B data sets for two exemplary months (February and August 2014).
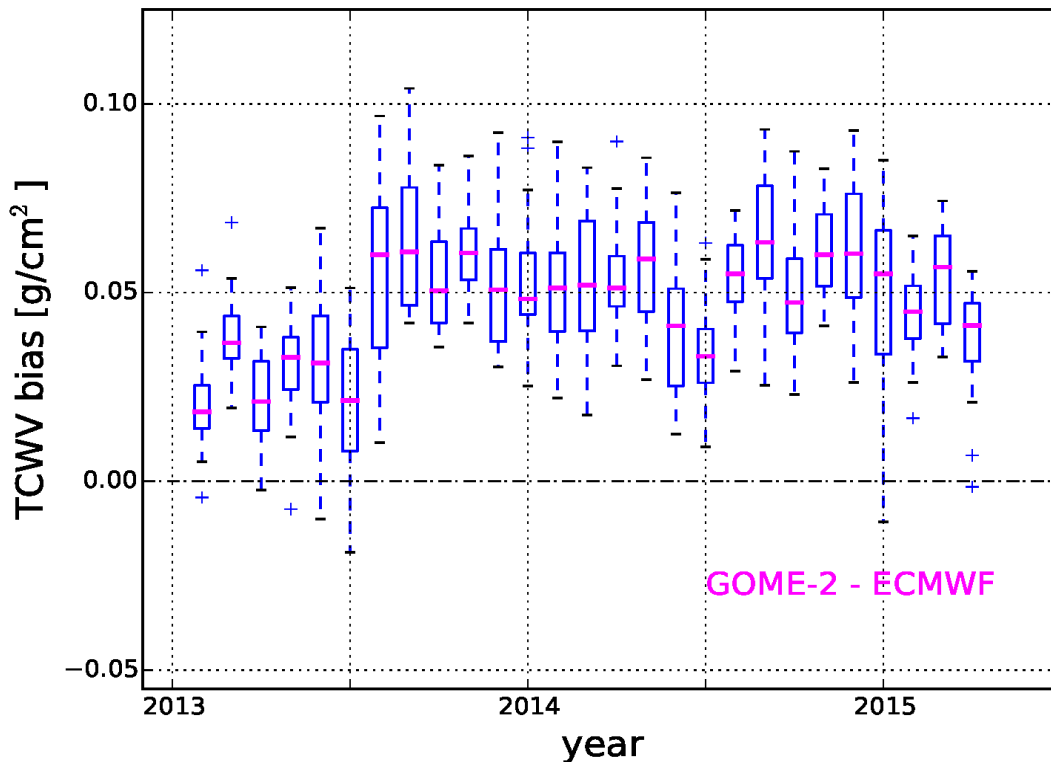
Figure 5.2: Global monthly median bias between ECMWF ERA-Interim model data and the combined GOME-2A and GOME-2B TCWV product (magenta lines).

5.3   Monthly comparison

In Figure 5.3 we present the monthly mean TCWV product in February 2014 obtained from daily co-locations of ECMWF ERA-Interim and GOME-2B data. We choose this month as representative of the water vapour distribution in the northern hemisphere winter season. In Figure 5.4, one can see the corresponding ECMWF ERA-Interim and GOME-2B measurements in August 2014. We studied daily co-locations (and not monthly data sets) in order to derive conservative estimates for the precision of our water vapour retrieval. This is important to remove part of the bias introduced by the presence of TCWV data retrieved in cloudy conditions in microwave measurements and simulated data. As already discussed in Section 2.3, for the comparison we used the ECMWF ERA-Interim 12 hour forecast based on 00 and 12 UTC analysis in order to have a more independent data set, since they include modeling. Looking at the monthly mean differences between GOME-2B and ECMWF ERA-Interim, we can distinguish only few regions with obvious discrepancies, e.g. the Amazon basin and sub-equatorial Africa in February 2014, or the south-east Asia in August 2014. Overall, we find similar spatial patterns in the H_2O distribution in the ECMWF ERA- Interim and GOME-2B data sets.
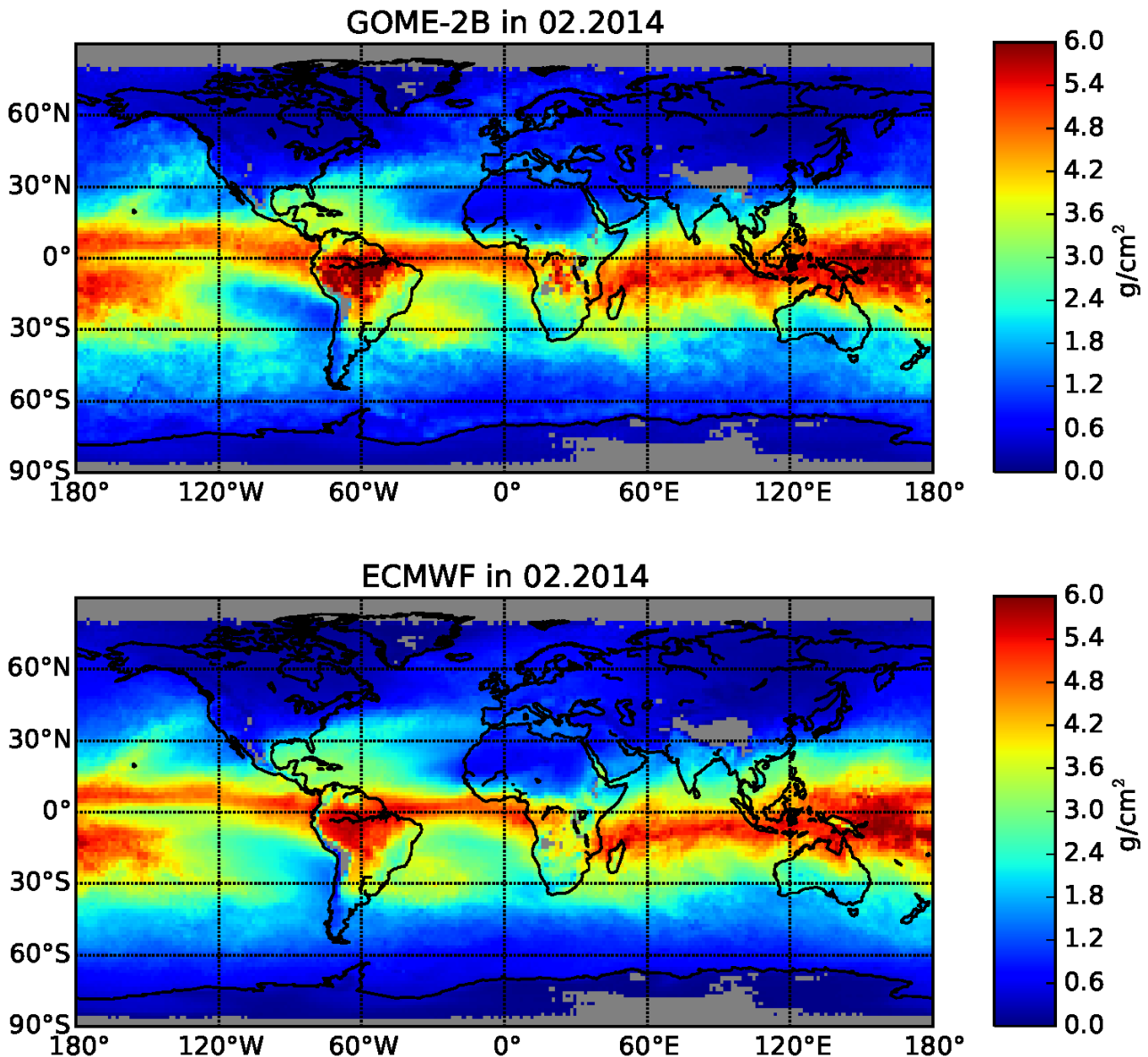
Figure 5.3: Global monthly mean maps of total column water vapour from GOME-2A (top panel) and ECMWF ERA-Interim (bottom panel) co-located data for February 2014. Only cloud-screened data have been used.

In order to quantify the discrepancies between ECMWF ERA-Interim data and the GOME-2 TCWV retrieval, in Figure 5.5 we show the spatial distribution of the bias for co-located and (mostly) cloud-free measurements in February 2014. The mean bias between ECMWF ERA-Interim and the GOME-2A and GOME-2B data sets is 0.047 g/cm² and 0.082 g/cm². We obtained very similar results when considering the ECMWF ERA-Interim analysis data set (slightly larger bias: 0.05 g/cm² and 0.085 g/cm² for GOME-2A and GOME-2B, respectively). Looking at the maps we can see that the bias is overall very low. Any deviation below the typical scatter of water vapour data of 0.4 g/cm² (i.e. the light red and light blue areas in the plot) can be considered as a good agreement. GOME-2 exhibits a number of dry and wet spots in south Africa and South America Amazonian regions, not visible in the ECMWF ERA-Interim product, which are probably related to the very low number of co-locations in these regions due to the cloud screening. Also, problems of

the ECMWF ERA-Interim data cannot be excluded, since remote regions may present larger errors due to paucity of observational information in the reanalyses, such as shown in Dee and Uppala (2009) for locations at latitudes greater than 70 degrees North. The differences along the ITCZ and the Pacific Warm Pool region, on the other hand, might be caused by the rather high cloud tops in these regions, leading to low measured AMF and consequently to rather high H_2O total columns. Even though we consider only grid boxes without severe cloud cover on a daily basis, some cloud effects are still present. Finally, we can remark that because GOME-2B operates on a wider swath than GOME-2A (1920 km instead of 960 km), the bias distribution appears to be smoother in this comparison (also the daily bias values have a smaller spread).
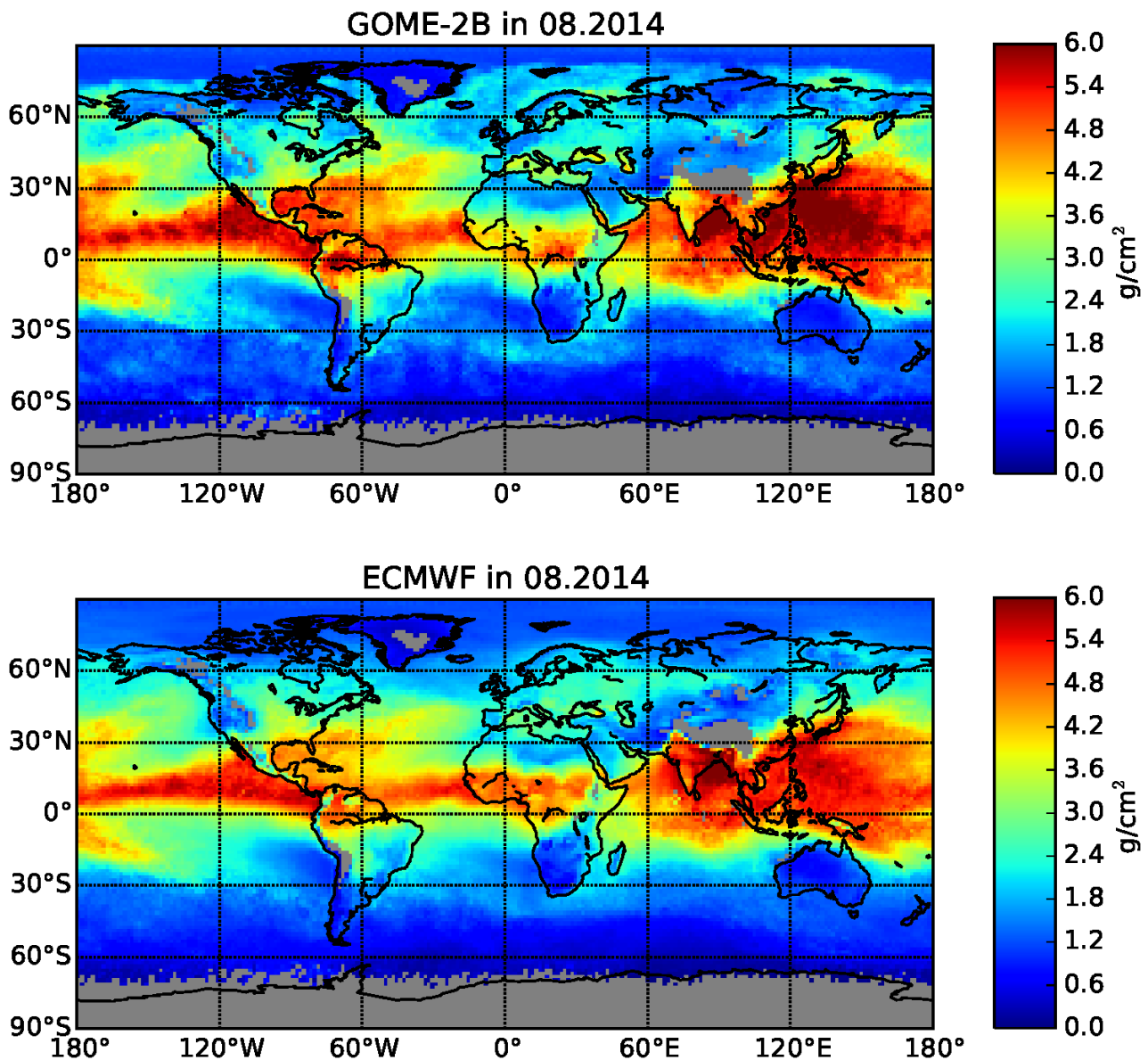
Figure 5.4: Global monthly mean maps of total column water vapour from GOME-2A (on the left) and ECMWF ERA-Interim (on the right) co-located data for August 2014. Only cloud-screened data have been used.

GOME-2A - ECMWF in 02.2014

GOME-2B - ECMWF in 02.2014
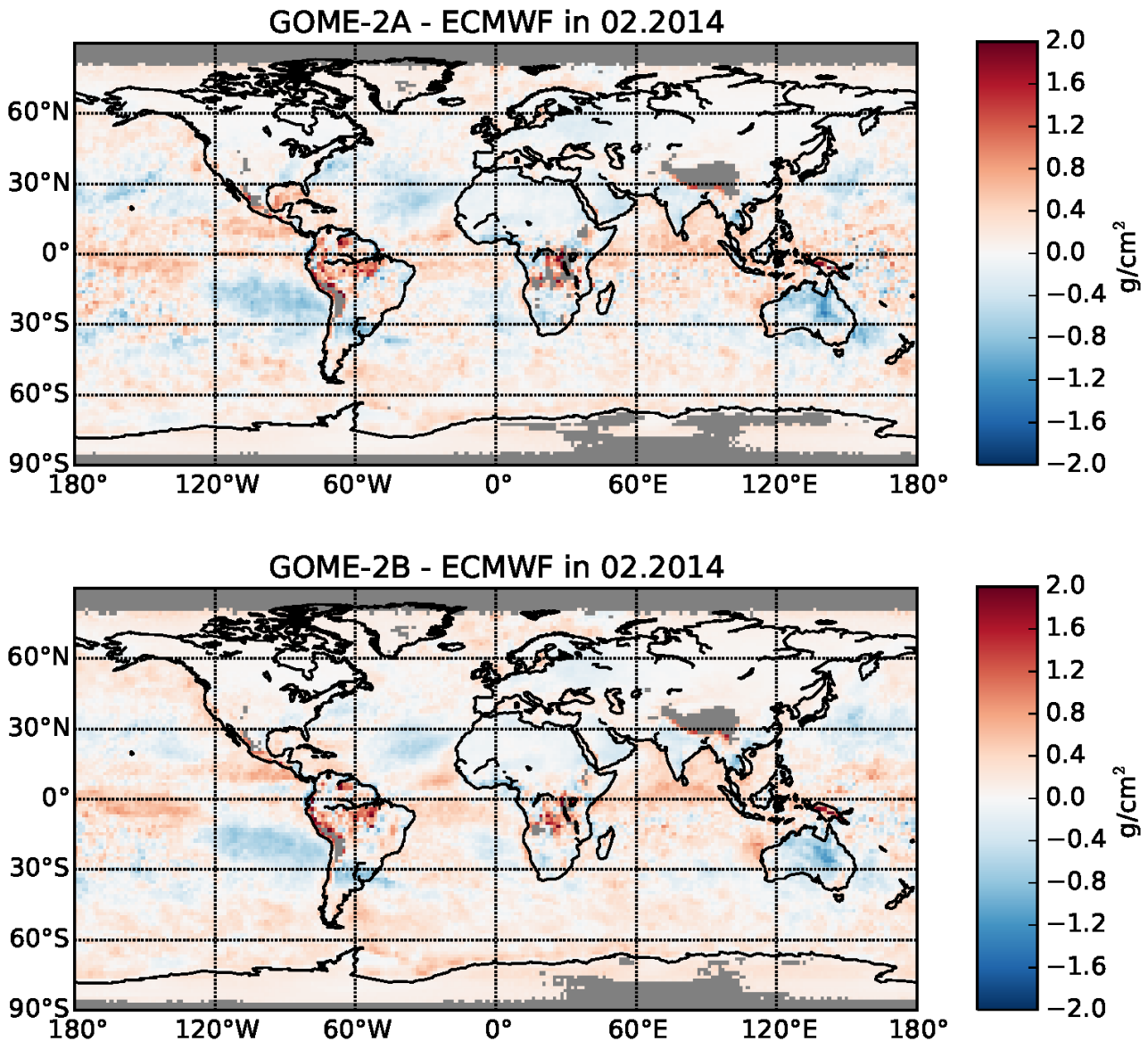
Figure 5.5: Geographical distribution of the differences between GOME-2A and ECMWF ERA-Interim TCWV (top panel) and GOME-2B and ECMWF ERA-Interim TCWV (bottom panel) in February 2014. Only cloud-screened co-located data have been used.

Relative large differences between the GOME-2 TCWV product and ECMWF ERA-Interim data can be seen in August 2014. The mean global bias is 0.064 g/cm² for GOME-2A and 0.102 g/cm² for GOME-2B (0.067 g/cm² for GOME-2A and 0.104 g/cm² for GOME-2B with respect to the analysis data set). As seen in Figure 5.6, the humidity in the Sahel/Sahara region is much lower in the GOME-2 data than the one estimated in the ECMWF ERA-Interim data (absolute and relative differences larger than −1 g/cm² and 20%, respectively). A negative bias can be observed in the region that goes from India till the east coast of China and reaches values between −1.5 g/cm² and −2.1 g/cm² in the northern part of the Indian Subcontinent. Looking at Figure 5.6, we can notice that the underestimation (blue regions denote negative bias) is located in land areas with a very high humidity in the northern hemisphere summer months. From a correlation analysis, we found that the bias between GOME-2A and ECMWF ERA-Interim data over land areas decreases (larger negative values) with increasing humidity. This is consistent with the results of the validation against ground-

based measurements (see Chapter 4). The same pattern in the bias distribution is observed for the comparison with respect to GOME-2B data.

Dry bias is observed also in arid areas, like southern regions of the Sahara desert, the coast of Somalia, the Arabian Desert in the Arabian Peninsula and the Thar desert in the northwestern part of the Indian Subcontinent. Regions with relatively high surface albedo values (in the range 0.3–0.5) which present dry bias include Northern Africa, the Arabian Peninsula, India and part of East Asia and Central America. A possible explanation for the discrepancies is that, because of absorbing aerosols over deserts, the surface albedo we measure there is lower than it's real value and, therefore, we underestimates the water vapour content (Fournier et al. 2006). However, the determination of the "real" surface albedo over desert regions is still a field of discussion, because of the uplifting of large amounts of dust, which lower the reflectivity (Herman et al., 1997; Torres et al., 1998).
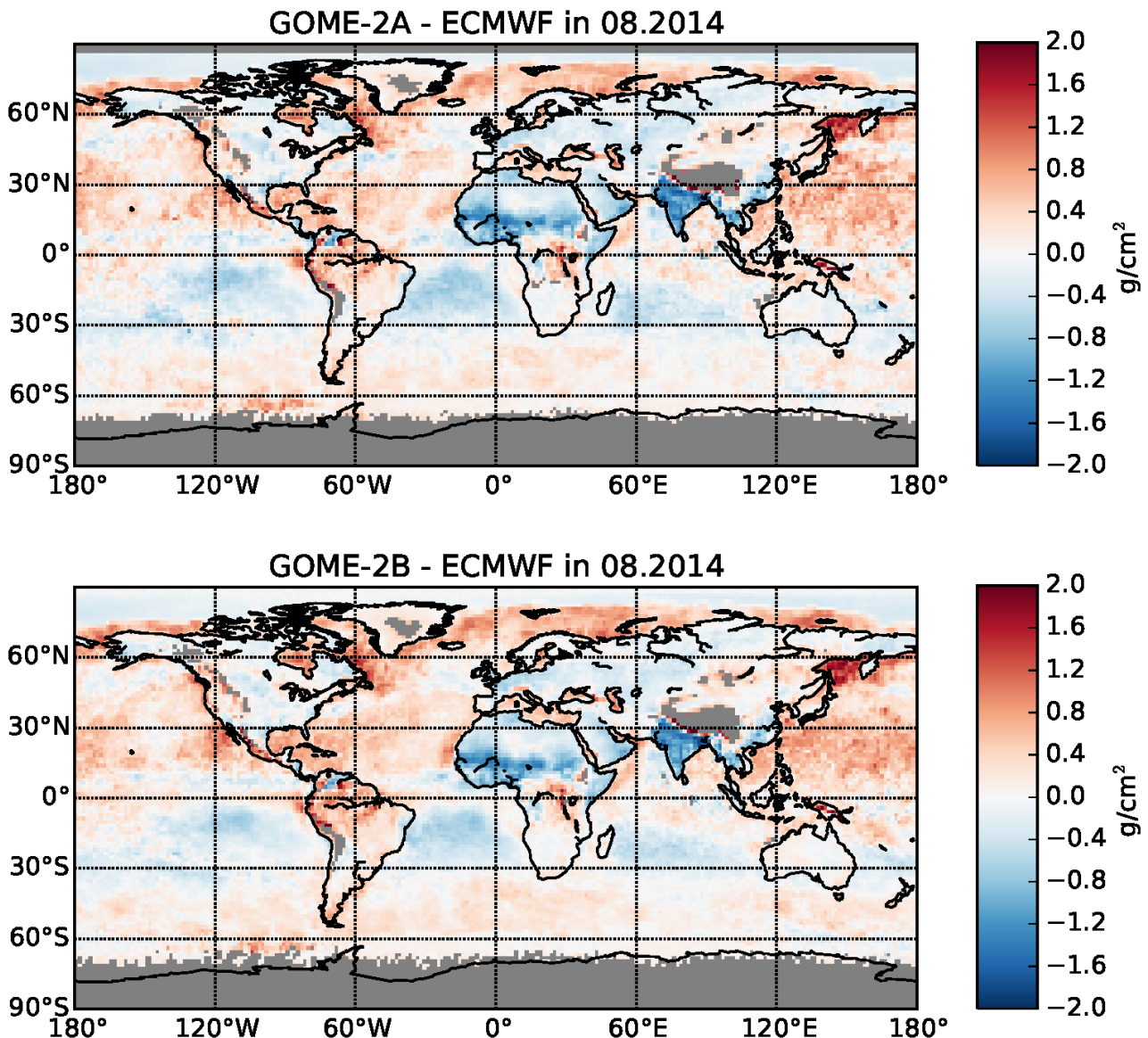
Figure 5.6: Geographical distribution of the differences between GOME-2A and ECMWF ERA-Interim TCWV (top panel) and GOME-2B and ECMWF ERA-Interim TCWV (bottom panel) in August 2014. Only cloud-screened co-located data have been used.
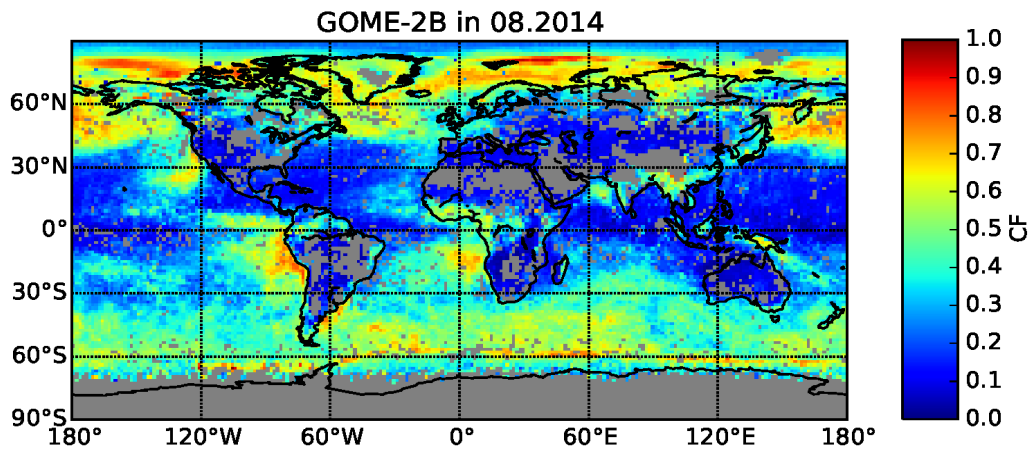
Figure 5.7: Geographical distribution of the residual cloud fraction in cloud-screened and co-located data used to evaluate the bias between GOME-2B and ECMWF ERA-Interim TCWV in August 2014. The cloud fraction is retrieved with the OCRA algorithm.

In the Northern Atlantic and in the Northern Pacific a strong wet bias between the GOME-2 and the ECMWF ERA-Interim measurements is observed in the summer months. The wet bias over ocean partly compensate the strong dry bias found over land regions reducing the global offset. Time lags between the two data sets may be critical, as water vapour is a rapidly varying atmospheric parameter, especially at high latitudes. However, the bias is mainly observed in regions with larger residual cloud fraction over ocean. The accuracy of TCWV retrieved with the UPAS algorithm is reduced by the presence of clouds that are not removed by the two cloud flagging criteria (see Section 2.1). In Figure 5.7 is shown the global distribution of the residual cloud fraction for cloud screened and co-located GOME-2B with ECMWF ERA-Interim data in August 2014.

Finally, we can remark that the biases we observe in the ECMWF ERA-Interim comparison are confirmed by a monthly comparison with IGRA radiosondes. However, the two data sets are not completely independent of each other. Observations assimilated in ERA-Interim consist of a large variety of in situ and satellite data, including radiosondes data and clear-sky radiances from SSM/I and SSMIS. Over land, a larger dry bias in the northern hemisphere summer months was found also when comparing GOME-2 with the combined SSM/I+MERIS data set derived within the ESA DUE GlobVapour project (Grossi et al., 2015).

6. COMPARISON WITH SSMIS TCWV

6.1 Method

In this study, we compare GOME-2A and GOME-2B H_2O VCDs with SSMIS results obtained from the F16 satellite from the Remote Sensing System (REMSS). We use daily average of the global H_2O total column observations for the period January 2007 to March 2015 for GOME-2A and from January 2013 to March 2015 for GOME-2B. We only use cloud-screened GOME-2 water vapour measurements over ocean.

The three data sets (SSMIS, GOME-2A and GOME-2B) are validated in different ways. The differences between the daily averaged global water vapour are investigated. To allow comparisons without over-weighting areas with a high density of co-locations, all the measurements have been binned into daily means on a grid of 1.5^O longitude x 1.5^O latitude. As in the comparison against ECMWF ERA-Interim data, maps of the bias between the monthly averaged H_2O VCDs are shown. More than eight years overlap between GOME-2A and SSMIS data provide also a very good opportunity to investigate the seasonal dependence of the results.

6.2 Global comparison

We perform comparisons between SSMIS and the three GOME-2 data sets (GOME-2A, GOME-2B and combined GOME-2A and GOME-2B products) for the time period January 2007- March 2015. Figure 6.1 shows the time series of the globally averaged bias derived from the monthly mean H_2O total column. The agreement between SSMIS data and the GOME-2 measurements is good for all comparisons: the mean biases for the full time series are in the range between 0.005 and 0.045 g/cm^2, while the Root Mean Square Error (RMSE) varies between a minimum of 0.26 and a maximum of 0.28 g/cm^2. Positive bias implies that the GOME-2 TCWV is slightly higher on average.

Further analysis of the GOME-2 and SSMIS intercomparison (blue line and points in Figure 6.1) evidentiate a seasonal dependence in the results. In all three data sets, the bias is high in the northern hemisphere summer and low in the northern hemisphere winter. The monthly averaged bias ranges from a minimum of -0.082 g/cm^2 in January 2010 (blue dots, GOME-2A - SSMIS) to a maximum of 0.132 g/cm^2 in July 2013 (green dots, GOME-2B – SSMIS). Large seasonal variations in the distribution of the mean bias are also visible when plotting the bias between GOME-2 and ECMF ERA-Interim data only over ocean. In the full data set, on the other hand, the seasonal dependence is not as evident as a results of the opposite bias over land and ocean surfaces (see Chapter 5).

Interpreting these results, we should have in mind the limitations of GOME-2 retrieval. Although a specific advantage of the visible spectral region is that it is sensitive to the water vapour concentration close to the surface and that it has the same sensitivity over land and ocean and can thus yield a consistent global picture, the accuracy of an individual observation is, in general, reduced for cloudy sky observations. Since the microwave instruments can measure the water vapour also below clouds, we expect some residual difference between GOME-2 data (based on visible observations, where cloud blocks the radiation) and SSMIS data, which deliver results also in cloud conditions. Therefore, a seasonal cycle of the geographic distribution of the bias could be caused, among other reasons, by the seasonality of cloud properties, as well as the variability of the

geographic distribution of major cloud structures as the Intertropical Convergence Zone (ITCZ). In addition, since GOME-2 observations are made at 9:30 LT, especially in regions with a pronounced diurnal cycle, they might not be representative for the daily, and therefore monthly, average TCWV.
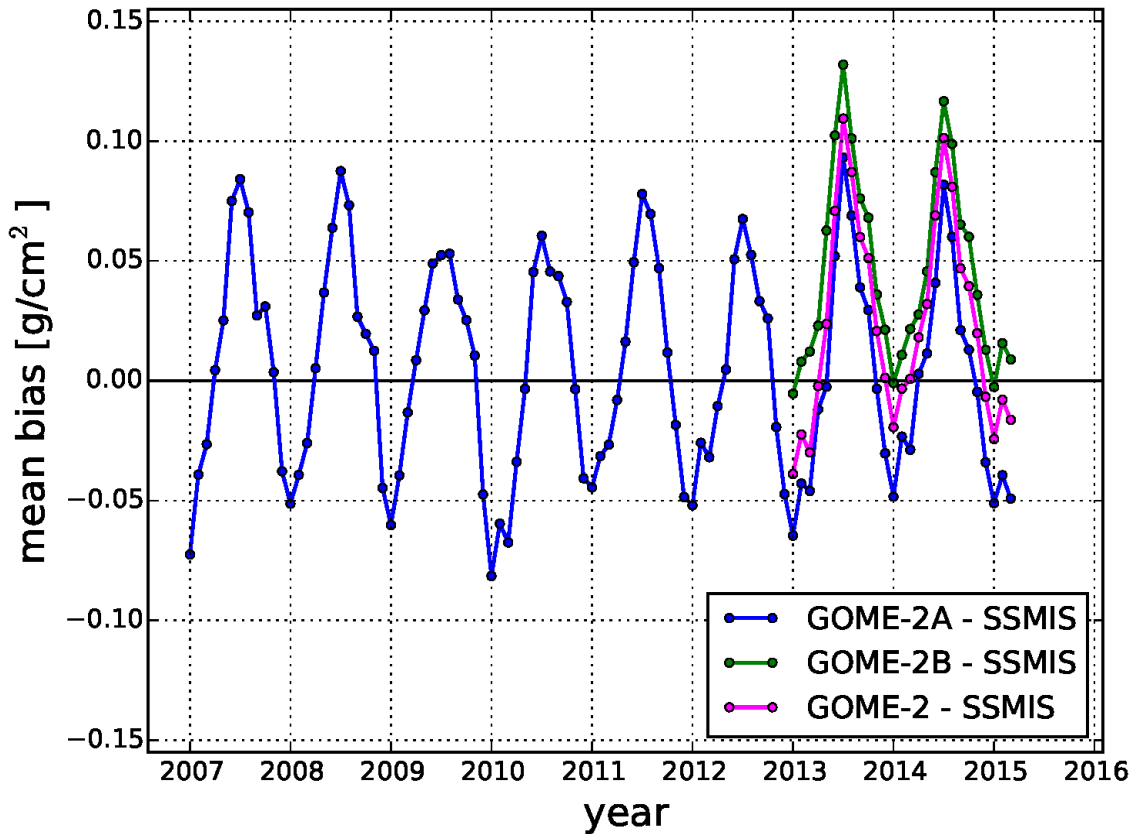
Figure 6.1: Global monthly mean bias between SSMIS data and GOME-2A TCWV (blue points), GOME-2B TCWV (green points) and combined GOME-2A and GOME-2B TCWV product (magenta points).

Table 6.1: Bias and RMSE statistics. The computations refer to the average difference GOME-2-SSMIS data. The time period analyzed is January 2007 – March 2015 for the comparison GOME-2A - SSMIS and January 2013 - March 2015 for GOME-2B – SSMIS and GOME-2 (combined GOME-A and GOME-2B data) - SSMIS.

Data	Bias (g/cm^2)	RMSE (g/cm^2)
GOME-2A - SSMIS (01.2007-03.2015)	0.005 +/- 0.044	0.280 +/- 0.048
GOME-2B - SSMIS (01.2013-03.2015)	0.046 +/- 0.039	0.281 +/- 0.051
GOME-2 - SSMIS (01.2012-03.2015)	0.025 +/- 0.042	0.264 +/- 0.051

A strong seasonal distribution can be observed also looking at the median of the monthly bias between the combined GOME-2 product and the SSMIS observations (see Figure 6.2, magenta lines). The median bias is very close to the mean results (only slightly smaller), with larger positive bias in the northern hemisphere summer months and lower bias in the northern hemisphere winter months.

As discussed before, the effect of performing a comparisons only over ocean measurments is to have a larger variations in the monthly values of the bias. On the other hand, the spread in the monthly data is relatively small (the bias is within 0.05 g/cm^2 in half of our daily measurements). The distribution of the bias values is moderately skewed towards positive values in the majority of the months.

In the next section we studying two exemplary months (February and August 2014) in order to study the differences in the TCWV distribution on a local scale.
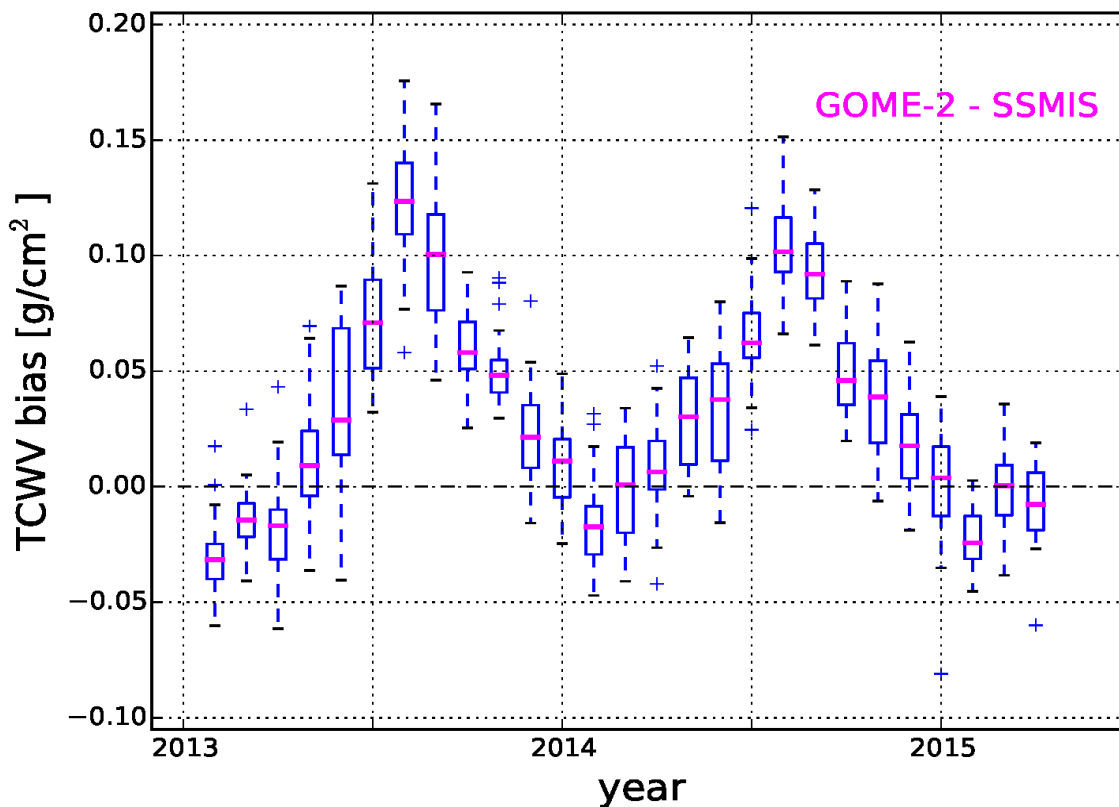
Figure 6.2: Global monthly median bias between SSMIS data and the combined GOME-2A and GOME-2B TCWV product (magenta lines).

6.3 Monthly comparison

Figure 6.3 and Figure 6.4 show the global monthly bias between GOME-2 and SSMIS observations in February and August 2014. The land regions are masked in the comparison, because the SSMIS data set is available only over ocean scenes, but microwave sensors can retrieve TCWV also in the presence of clouds and for night time satellite overpasses. We used outputs from the ascending and descending F16 orbit from the daily binary SSMIS data files in order to compute gridded daily mean data used for co-locations. Ascending local equator crossing time is 16:39 LT as of 16 October 2014, and descending time 4:39 LT. If we evaluate the bias between GOME-2 and SSMIS from monthly mean data, we would find a larger and negative bias because of the cloud influence. Thus, as for ECMWF ERA-Interim data, we select only daily co-locations and we reject the SSMIS data if the corresponding GOME-2 measurement is contaminated by clouds. This selection minimizes the effect of temporal change and cloud contamination in the GOME-2 vs SSMIS comparison. The number of co-locations is further reduced since the TCWV retrieval is not possible in situations with high precipitation or near land areas (< 25 km).

In February 2014, the bias between GOME-2A and SSMIS is small and negative (-0.023 g/cm^2). Looking at the top panel of Figure 6.3, we observe very small discrepancies for most ocean regions. As expected, since the GOME-2B data are wetter than the GOME-2A data, the mean bias is slightly positive in this case (0.011 g/cm^2) and reaches values up to ±0.5 g/cm^2 in some costal areas, like the western coast of Australia and north America. The same patterns in the bias distribution are visible in the GOME-2A and GOME-2B data set.

We retrieve a larger mean bias of about 0.06 g/cm^2 and 0.09 g/cm^2 in August 2014 for the comparison GOME-2A - SSMIS and GOME-2B - SSMIS, respectively. Looking at Figure 6.4, a large positive bias is clearly visible in regions at high latitude, in particular the northern areas of the Atlantic and Pacific ocean. At northern latitudes (45 - 75 degree north) the bias typically ranges between 0.1 and 0.62 g/cm^2, but more than 5% of the map bins have values more than 1 g/cm^2. These areas are the dominating cause for the pronounced seasonal component in the SSMIS against GOME-2 comparison results. The same differences were also observed in the comparison with the ECMWF ERA-Interim data set (see Figure 5.6) and are thus likely related to the GOME-2 measurements and associated with higher cloud fraction values (> 0.5). In Figure 6.5 we report the global distribution of the cloud fraction in the co-located data in August 2014. Residual cloud contamination is visible especially in the Bering Sea and in the northern coast of the european continent. Intermediate values of cloud fraction are found at high latitudes and in the Southern Ocean.

Among the limitations of the SSMIS data, on the other hand, we should mention that the model and algorithm for the retrieval are calibrated using an in-situ database containing overpasses of buoys and radiosonde sites. The accuracy of the TCWV product depends on the quality of these observations, and not all the regions and atmospheric situations may be equally represented in the training data set (Andersson et al., 2010). It was already shown that the maximum bias between satellite and ship data (of about 0.25 g kg^{-1}; average bias of approximately 2%) was found precisely over the North Atlantic Ocean during the summer season (Bentamy et al., 2003). Also, depending on location and season, systematic differences of atmospheric humidity of about 1% for 1 hour time difference between the GOME-2A and SSMIS retrieval might be expected (Kalakoski et al., 2011), and in regions with a particularly high diurnal variability, as for instance over the North Atlantic, they can be even larger.
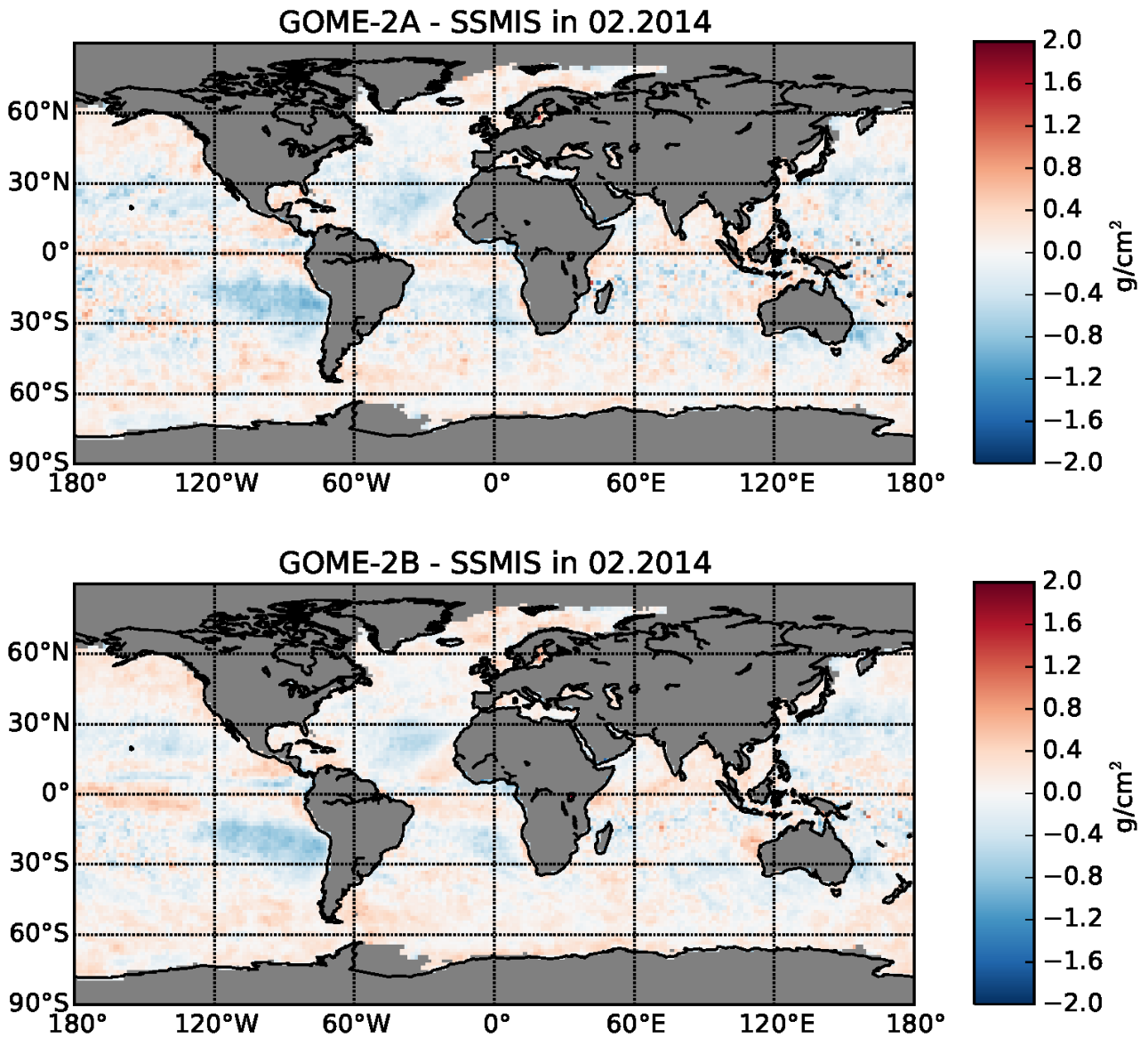
Figure 6.3: Geographical distribution of the differences between GOME-2A and SSMIS TCWV (top panel) and GOME-2B and SSMIS TCWV (bottom panel) in February 2014. Only cloud-screened co-located data have been used.
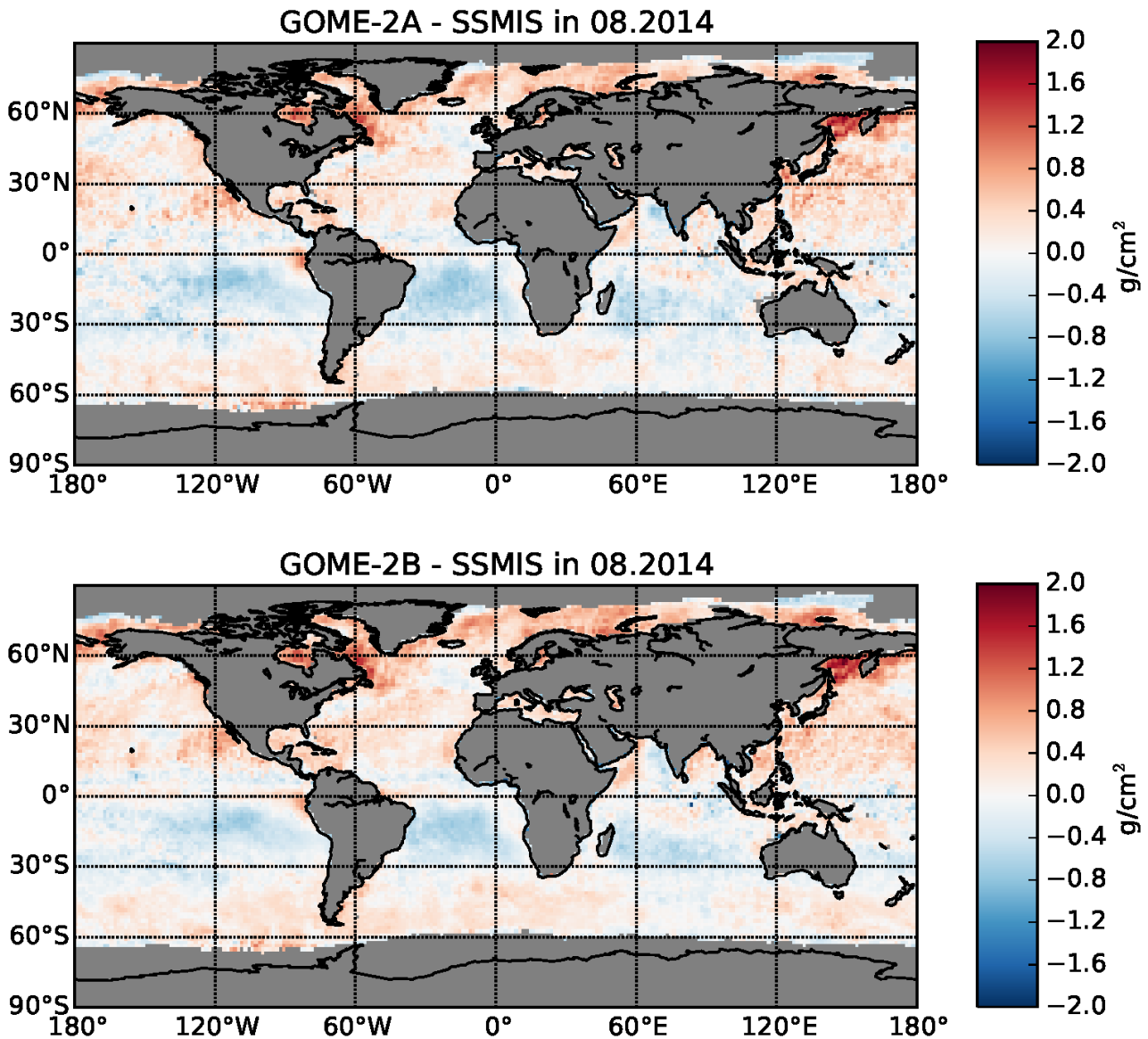
Figure 6.4: Geographical distribution of the differences between GOME-2A and SSMIS TCWV (top panel) and GOME-2B and SSMIS TCWV (bottom panel) in August 2014. Only cloud-screened co-located data have been used.

An orthogonal regression analysis of GOME-2A against SSMIS (Figure 6.6) shows a very good correlation between the two data sets with a slope very close to 1 (0.93) and a negative offset of about -0.4 g/cm^2, which is compatible with the negative mean bias (see Table 6.1). Figure 6.7 shows the scatter plot and histogram of the GOME-2B total column as a function of the SSMIS water vapour results. We obtained similar results with respect to the GOME-2A sample in Figure 6.6, with a slightly bigger slope (0.94) and offset. The difference and standard deviations are also comparable. The validation between SSMIS and the GOME-2B water vapour column further consolidate the findings of the GOME-2A - GOME-2B comparison, with mean bias within the optimal accuracy range (5%) as stated in the O3M SAF [PRD].
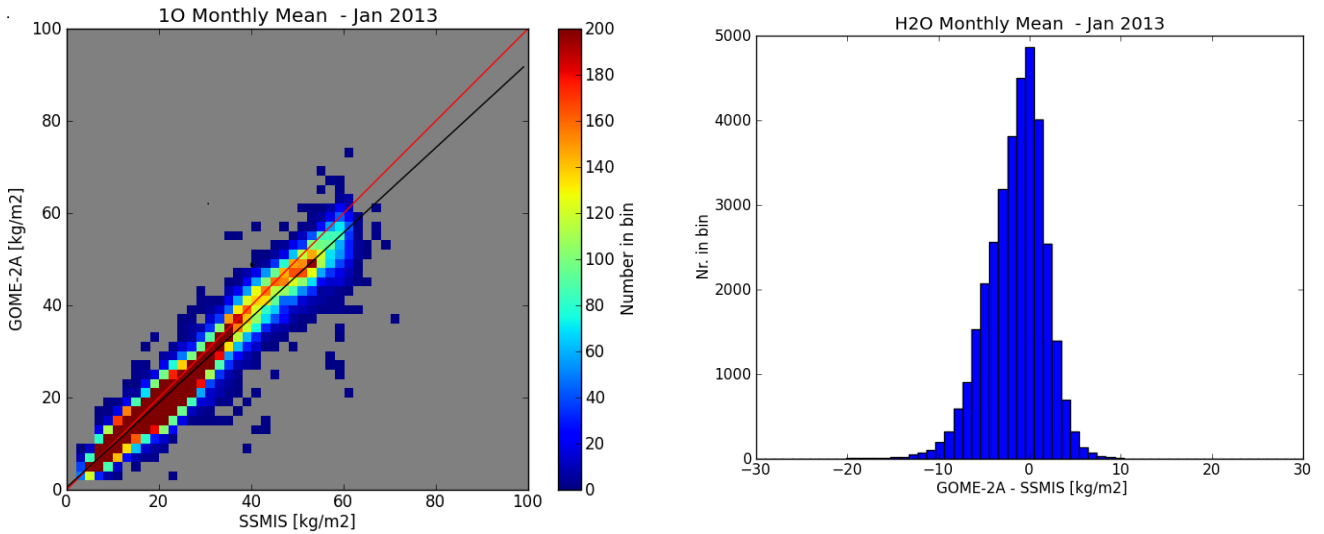
Figure 6.6: Left panel: scatter plot of GOME-2A monthly mean total columns against SSMIS monthly mean total columns, for January 2013. Clear-sky cases. Right panel: histogram of the difference GOME-2A - SSMIS, for the points in the scatter plot.
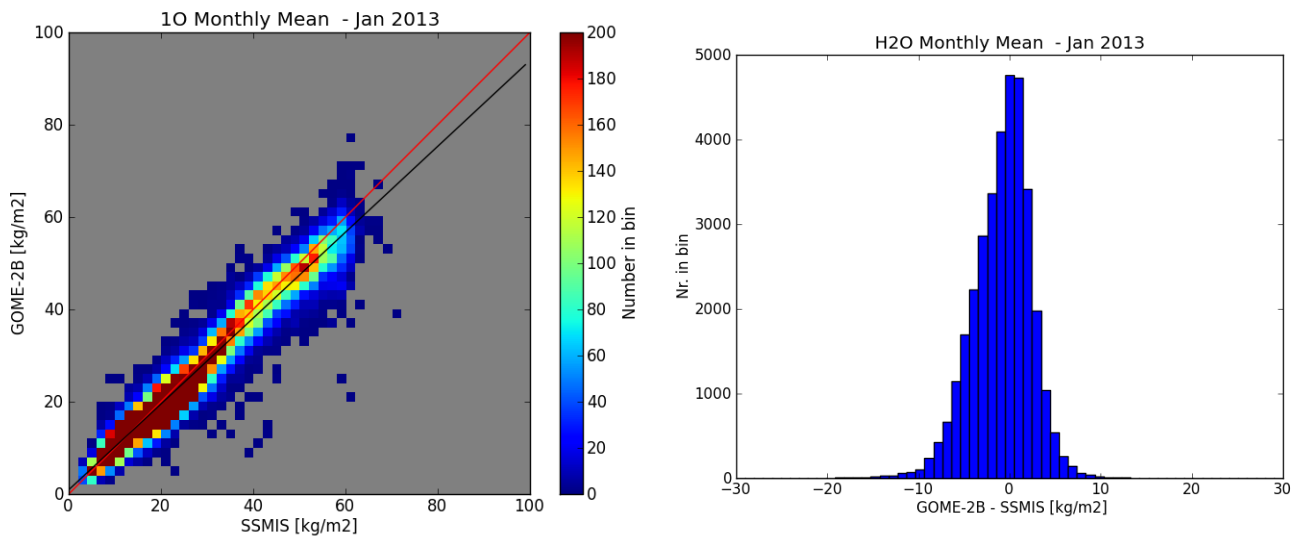
Figure 6.7: Left panel: scatter plot of GOME-2B monthly mean total columns against SSMIS monthly mean total columns, for January 2013. Clear-sky cases. Right panel: histogram of the difference GOME-2B - SSMIS, for the points in the scatter plot.
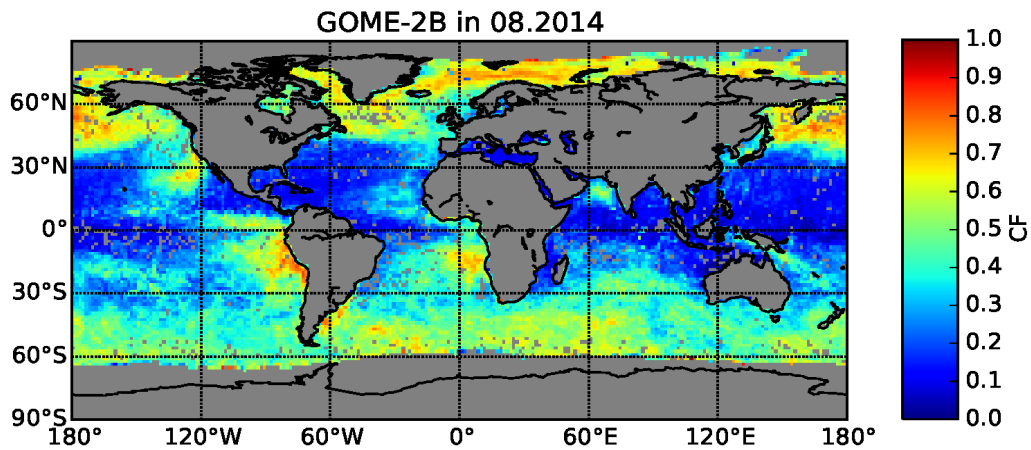
Figure 6.5: Geographical distribution of the residual cloud fraction in cloud-screened and co-located data used to evaluate the bias between GOME-2B and SSMIS TCWV in August 2014. The cloud fraction is retrieved with the OCRA algorithm.

7. CONCLUSIONS

This document reports on the validation of offline and reprocessed GOME-2/MetOp-A and GOME-2/MetOp-B (GOME-2B) H_2O column data generated at DLR using the level-1-to2 GOME Data Processor (GDP) version 4.8 and recorder over the time period January 2007-March 2015 and December 2012 through March 2015, respectively. Water vapour total columns have been evaluated using comparisons with (1) ground-based observations obtained from the IGRA radiosonde data set and GPS observations from the COSMIC/SuomiNet network, (2) model data from the ECMWF ERA-Interim reanalysis and (3) independent SSMIS F16 satellite measurements from the Remote Sensing System (REMSS). Moreover, an inter-comparison between GOME-2A and GOME-2B data in the period January 2013 to March 2015 is performed.

Each of these data sets has its own advantages and disadvantages. From the different comparisons, different properties of the GOME-2 data set can be studied.

The inter-comparison between GOME-2B water vapor VCDs with GOME-2A observations is possible over both land and ocean with similar coverage. Since the algorithm used for the retrieval of H_2O total columns is the same, this comparison allows investigating the internal consistency between results from both sensors during the overlap period. The validation of GOME-2 water vapour VCDs versus radiosonde data yields mainly information over land, but also some data over ocean are available. Nevertheless, the spatial distribution of the radiosonde data is not homogeneous and thus only limited spatial patterns can be gained. Radiosonde measurements can be performed independently on cloud cover, thus information on the dependence of GOME-2 water vapour VCDs on cloud properties can be derived. ERA-Interim represents a major undertaking by ECMWF to produce a reanalysis with an improved atmospheric model and assimilation system and has the advantage of providing global data at high spatial and temporal resolution and being suitable for studies of long-term atmospheric variability. The comparison of GOME-2 H_2O columns versus SSMIS observations, on the other hand, is restricted to measurements over ocean. SSMIS observations are independent of cloud cover and have also a good spatial coverage; thus we can derive information on spatial patterns in the differences between both data sets.

In the following, the main findings from the different comparison studies are summarised. More details can be found in the respective Sections.

From the intercomparison between GOME-2A and GOME-2B data, overall a very good consistency is found. The GOME-2A water vapour total columns are only slightly drier than the GOME-2B measurements and present a small, negative bias of about -0.037 g/cm^2 (less than 1 %), when averaging all the results for the January 2013 - March 2015 period. In the large majority of cases (> 90% of the time), the relative differences between GOME-2A and GOME-2B H_2O product are within 0.5 g/cm^2 in absolute value. The results do not change substantially whether we take into account co-located observations or all measurements.

Comparison with soundings and GPS observations show that both GOME-2A and GOME-2B observations are in good agreement with ground-based observations for water vapour amounts below 5 g/cm^2. For very large water vapour columns, both GOME-2 instruments underestimate the ground-based observations. Long-term comparisons show that the product is very stable over validation period (2007-2015). Some seasonal and latitudinal variation was also observed.

Both the GOME-2A and GOME-2B data are in good agreement with the SSMIS measurements. We found biases between -0.08 g/cm^2 and 0.13 g/cm^2 for the GOME-2 instruments in the full period January 2007 – April 2013 and correlation coefficient between GOME-2 and SSMIS data sets close to 1 (between 0.9 and 0.95). The comparison between GOME-2 and SSMIS data also revealed a

seasonal cycle in the geographical distribution of the bias, with a positive bias in June-August and a larger negative bias in December-January. The dominating cause for this pronounced seasonal component is a large positive bias in regions at high latitude, in particular the northern areas of the Atlantic and Pacific Ocean (bias values typically ranges between 0.1 and 0.62 g/cm^2). These variations can mainly be related to the impact of clouds on the accuracy of the GOME-2 observations and to the different sampling statistics of the instruments.

Finally, the ECMWF ERA-Interim data set are typicall slightly drier than the GOME-2 retrievals. On average GOME-2 data overestimate the ERA-Interim reanalysis by only 0.34 g/cm^2 (GOME-2A) and 0.067 g/cm^2 (GOME-2B). The seasonal behaviour is not as evident when comparing GOME-2 TCWV to the ECMWF ERA-Interim data sets, since the different biases over land and ocean surfaces partly compensate each other. Studying two exemplary months, we estimate regional differences and identify a very good agreement between GOME-2 total columns and ECMWF model data in February and August 2014, although some discrepancies (bias larger than 0.5 g/cm^2) over ocean and over land areas with high humidity or a relatively large surface albedo are observed.

Based on the intercomparison with GOME-2A water vapour VCDs and the validation with ground-based measurements and SSMIS monthly averaged data, we conclude that the current GOME-2/MetOp-B H_2O product fulfils the user requirements in terms of accuracy for most conditions (especially for climatologically relevant data), as stated in the Product Requirements Document (Optimal accuracy 5%; Target accuracy 10%; Threshold accuracy 25%) [PRD] .

8. REFERENCES

8.1 Applicable documents

ATBD Algorithm Theoretical Basis Document for GOME-2 Total Column Products of Ozone, NO2 , SO2, BrO, H2O, HCHO and Cloud Properties, DLR/GOME-2/ATBD/01, Rev. 3/A, P. Valks et al., March 2015.

PUM Product User Manual for GOME-2 Total Columns of Ozone, NO2, SO2, BrO, H2O, HCHO, and Cloud Properties, DLR/GOME-2/PUM/01, Rev. 3/A, Valks, et. al., 2015.

PRD O3M SAF Product Requirements Document, SAF/O3M/FMI/RQ/PRD/001/Rev. 1.7, J. Hovila, et. al., 2015.

SSD O3M SAF Service Specification Document, J. Hovila, S. Hassinen; http://o3msaf.fmi.fi/docs/O3M_SAF_Service_Specification.pdf

8.2 Reference documents

Andersson, A., Fennig, K., Klepp, C., Bakan, S., Grassl, H., and Schulz, J.: T*he Hamburg Ocean Atmosphere Parameters and Fluxes from Satellite Data - HOAPS-3*, Earth Syst. Sci. Data, 2, 215-234, 2010

Bentamy, A., K. B. Katsaros, A. M. Mestas-Nunez, W. M. Drennan, B. E. Forde, and H. Roquet: *Satellite estimates of wind speed and latent heat flux over the global oceans*. J. Climate, 16, 637–655, 2003

Bovensmann, H., Burrows, J. P., Buchwitz, M., Frerik, J., No¨el, S., Rozanov, V. V., Chance, K. V., and Goede, A.: *SCIAMACHY – mission objectives and measurement modes*, J. Atmos. Sci., **56**(2), 127–150, 1999

Burrows, J. P., Weber, M., Buchwitz, M., Rozanov, V., Ladstätter-Weißenmayer, A., Richter, A., de Beek, R., Hoogen, R., Bramstedt, K., Eichmann, K.-U., Eisinger, M., and Perner, D.: *The Global Ozone Monitoring Experiment (GOME): Mission Concept and First Scientific Results*, J. Atmos. Sci.,**56**, pp 151–175, 1999

Cox C, Munk W. *Measurement of the roughness of the sea surface from photographs of the Sun's glitter.* J Opt Soc Am; **44**(11): 838–50, 1954

Dee, D. P. and Uppala, S.: *Variational bias correction of satellite radiance data in the ERA-Interim reanalysis*. Q.J.R. Meteorol. Soc., 135: 1830–1841. doi: 10.1002/qj.493, 2009

Dee, D. and Coauthors: *The ERA-Interim reanalysis: Configuration and performance of the data assimilation system*. Quart. J. Roy. Meteor. Soc., 137, 553-597, 2011a

Dee, D. and Coauthors: *The use of reanalysis data for monitoring the state of the climate* [in "The State of the Climate in 2010"]. Bull. Amer. Meteor. Soc. 92(6), S34-S35, 2011b

Durre, I., R. S. Vose, and D. B. Wuertz: *Overview of the Integrated Global Radiosonde Archive*. J. Climate, **19**, 53-68, 2006

Grzegorski, M.: *Cloud retrieval from UV/VIS satellite instruments (SCIAMACHY and GOME)*, PhD thesis, University of Heidelberg, 2009

Grossi, M., Valks, P., Loyola, D., Aberle, B., Slijkhuis, S., Wagner, T., Beirle, S., and Lang, R.: *Total column water vapour measurements from GOME-2 MetOp-A and MetOp-B*, Atmos. Meas. Tech., 8, 1111-1133, doi:10.5194/amt-8-1111-2015, 2015

Kalakoski, N., T. Wagner, K. Mies, S. Beirle, S.Slijkhuis, D. Loyola: *O3M SAF Validation Report, Offline Total Water Vapour*, SAF/O3M/FMI/VR/H2O/111, 2011

Kalakoski , N., Kujanpää, J,. Sofieva, V,. Tamminen, J., Grossi, M., and Valks, P.: *Comparison of GOME-2/MetOp total column water vapour with ground-based and in-situ measurements*, amt-2014-292, 2014

Koelemeijer, R. B. A., Haan, J. F. D., and Stammes, P.: *A database of spectral surface reflectivity in the range 335–772 nm derived from 5.5 years of GOME observations*, J. Geophys. Res.,108(D2), 4070 , doi:10.1029/2002JH002429, 1650, 1651, 2003

Lang, R., Casadio S., Maurellis, A.N., and Lawrence M.G.: *Evaluation of the GOME Water Vapor Climatology 1995-2002*, J. Geophys. Res. **112**, D12110, doi:10.1029/2006JD008246, 2007

Loyola D., Thomas W., Livschitz Y., Ruppert T., Albert P., Hollmann. R.: *Cloud properties derived from GOME/ERS-2 backscatter data for trace gas retrieval*, IEEE Transactions on Geoscience and Remote Sensing, vol. 45, no. 9, pp. 2747-2758, 2007

Loyola D., Thomas W., Spurr, R., B. Mayer: *Global patterns in day-time cloud properties derived from GOME backscatter UV-VIS measurements*, International Journal of Remote Sensing, vol. 31, no. 16, pp. 4295-4318, 2010

Lutz, R., D. Loyola, S. Gimeno Garcia, F. Romahn: *OCRA radiometric cloud fractions for GOME-2A/B*, Atmos. Meas. Tech., to be submitted, 2015.

Noël, S., Mieruch S., Bovensmann, H., and Burrows, J. P.: *Preliminary results of GOME-2 water vapour retrieval and first applications in polar regions*. Atmos. Chem. Phys. **8**, pp 1519-1529, 2008

Wentz F. J., *A well-calibrated ocean algorithm for SSM/*I, J. Geophys. Res., Vol. **102**, No. C4, pg. 8703-8718, 1997

Wagner, T., Heland, J., Zoeger, M., and Platt, U.: *A fast H₂O total column density product from GOME – Validation with in-situ aircraft measurements*, Atmos. Chem. Phys., **3**, 651–663, 2003

Wagner, T., Beirle, S., Grzegorski, M., and Platt, U.: *Global trends (1996–2003) of total column precipitable water observed by Global Ozone Monitoring Experiment (GOME) on ERS-2 and their relation to near-surface temperature*, J. Geophys. Res. **111***, D12102, doi:10.1029/2005JD006523, 2006

Wentz, F.J.: *A well-calibrated ocean algorithm for SSM/I*, J.Geophys.Res. 102, No. C4, pp. 8703-8718, 1997

Wentz, F. J.: *SSM/I Version-7 Calibration Report*, report number 011012, Remote Sensing Systems, Santa Rosa, CA, 46pp, 2013